



Royal Netherlands Institute for Sea Research

This is a postprint of:

Gerringa, L.J.M.; Slager, H.A.; Bown, J.; van Haren, H.; Laan, P.; de Baar, H.J.W. & Rijkenberg, M.J.A. (2017). Dissolved Fe and Fe-binding organic ligands in the Mediterranean Sea – GEOTRACES G04. *Marine Chemistry*, 194, 100-113

Published version: <https://dx.doi.org/10.1016/j.marchem.2017.05.012>

Link NIOZ Repository: www.vliz.be/nl/imis?module=ref&refid=288511

[Article begins on next page]

The NIOZ Repository gives free access to the digital collection of the work of the Royal Netherlands Institute for Sea Research. This archive is managed according to the principles of the [Open Access Movement](#), and the [Open Archive Initiative](#). Each publication should be cited to its original source - please use the reference as presented.

When using parts of, or whole publications in your own work, permission from the author(s) or copyright holder(s) is always needed.

Dissolved Fe and Fe-binding organic ligands in the
Mediterranean Sea – GEOTRACES G04

L.J.A. Gerringa, H.A. Slagter, J. Bown, H. van Haren, P. Laan, H.J.W. de Baar,
M.J.A. Rijkenberg

NIOZ Royal Netherlands Institute for Sea Research, Department of Ocean Systems (OCS), and Utrecht University, P.O. Box 59, 1790 AB Den Burg, Texel, the Netherlands

Marine Chemistry: 10.1016/j.marchem.2017.05.012

Abstract
Dissolved Fe (DFe) and Fe-binding dissolved organic ligands were analysed during two GEOTRACES cruises in the Mediterranean Sea in May and August 2013.

DFe was relatively high near the surface probably due to atmospheric sources, whereas below 500-700 m depth the concentrations were relatively low, <0.4 nM, compared to typical concentrations of 0.6 nM at the same depths in the Atlantic Ocean. These relatively low concentrations are probably due to scavenging and ballasting by dust particles settling down through the water column. Especially in the Eastern Basin, and more prominent in its northern part, distinct patches with high DFe, up to 8.40 nM, were found between 200 and 3000 m depth. These patches were local, which indicates a point source and lateral transport from this source. Some of these patches coincided with sloping density lines indicating enforced along-frontal currents providing lateral transport of DFe. Sources are probably seamounts and mud volcanoes, which were found to exist at the same depths as the elevated DFe. It is conceivable that a large eddy keeps infusions of DFe isolated from mixing with other water masses. These infusions could originate from slopes or from downwards cascading materials out of canyons.

Fe-binding dissolved organic ligands increase the solubility of Fe enabling high dissolved Fe concentrations, and hence longer residence time. These ligands had median total concentrations between $[Lt]=0.77$ and $[Lt]=1.74$ nEq of M Fe and conditional stability constants between $\log K'=21.57$ and $\log K'=22.13$ ($N=156$). Median values of $[Lt]$ were higher in the upper 100 m and its median concentration increased from west to east. The $[Lt]$ concentrations did not relate to water mass or DFe concentration. The ligands were nearly saturated with Fe where DFe was elevated near the surface and completely saturated, ratio $[Lt]/DFe \leq 1$, in patches with high DFe at depth. The high DFe concentrations in these patches are extreme, if not even maximum, concentrations as any surplus Fe with respect to the ligands will tend to precipitate. Calculated inorganic Fe concentrations in the Mediterranean had minimum concentrations of 0.23 pM and below 100 m depth median concentrations that varied between 0.68 and 1.99 pM only. This suggests that the inorganic Fe concentration is the result of a steady state between binding by organic ligands and scavenging processes. Thus scavenging will not result in lower inorganic Fe concentrations and in this way the dissolved ligand concentration determines the concentration of DFe in the Mediterranean Sea.

Keywords: GEOTRACES, dissolved Fe, organic ligands, Mediterranean Sea, dust, Fe speciation.

1. Introduction

The Mediterranean Sea is surrounded by land and this has a strong influence on the chemical composition of the water and mixing processes therein. It has a surface area of about 2.5 million km² and a mean depth of 1500 m, with typical basin depths of 3000 m, while maximum depths exceed 5000 m in its Eastern Basin. In the west, the Mediterranean is connected with the Atlantic Ocean by the Strait of Gibraltar which is 14.3 km wide and has a sill depth of 280 m. The Western and Eastern Basins are divided by the Sicily Strait, with a sill depth of 316 m. In that region and further into the Eastern Basin, volcanic and hydrothermal activities are abundant. In the east, the Mediterranean is connected with the Black Sea via the Sea of Marmara, (average depth 490 m) and the Channel of the Bosphorus (31 km long, 3 km wide, and an average midstream depth of 64 m). These narrow and shallow connections with the Atlantic Ocean and the Black Sea, in combination with high net evaporation, result in the high salinity in the Mediterranean, $38 < S < 39$. The Eastern Basin is warmest and most saline.

Near-surface, upper 300 m circulation of relatively fresh Atlantic Water is counter-clockwise (cyclonic) (e.g., Millot, 1999; Millot and Taupier-Letage, 2005). This basin-scale circulation along the continents is unstable, resulting in smaller, 100 km diameter spin-off meso-scale eddies. These eddies are mostly found in the southern part of the basins. They are most intense in the upper 200 m with horizontal speeds up to 1 m s^{-1} , but can reach the basin floor where they have horizontal speeds of typically 0.05 m s^{-1} . These eddies can quickly transport dissolved and particulate materials into the deep through vertical speeds of 0.01 m s^{-1} , being approximately 1000 m per day (van Haren et al., 2006). Another even faster vertical transport process occurs in the northern part of the Mediterranean, being one of the few regions outside of the polar oceans where dense water formation occurs (Voorhis and Webb, 1970; Gascard, 1973). Due to cooling and evaporation by continental winds in winter, surface waters can become denser than underlying waters so that they sink by turbulent, natural convective mixing in 0.1-1 km wide ‘chimneys’. The chimneys themselves are part of sub-mesoscale eddies (Testor and Gascard, 2003), which further mix newly formed deep dense waters with overlying water masses with the aid of the Earth rotation (van Haren and Millot, 2009). In the Mediterranean, this mainly occurs in the northern part of the Western Basin and in the Adriatic Sea of the Eastern Basin. This process occurs every year reaching depths of several hundreds of meters, but roughly every 8 years it reaches all the way to the bottom. More rarely, every few decades, formation of deep dense water occurs in the Aegean Sea (Roether et al., 2007).

The influence of the surrounding continents on the chemistry of the Mediterranean is relatively large. In this study we focus on dissolved Fe (DFe). Rivers like the Nile and the Rhone are sources of dissolved and particulate matter. It is assumed that the influence of rivers as source of metals like Fe to seas and oceans is modest, since flocculation within the estuarine zone will remove the majority of these metals (Sholkovitz, 1976; 1993; Boyle et al., 1977; Dai et al., 1995; Paucot and Wollast, 1997; Tachiwaka et al., 2004). However, lateral transport of DFe is known to reach very large distances of 1000 km or more in the upper 200 m (De Jong et al., 2012; Rijkenberg et al., 2012) and in the deep ocean (Fitzsimmons et al., 2014). Moreover, nepheloid layers originating from shelves can occasionally cascade down canyons and cover the whole bottom of the Western Basin (Puig et al., 2013) and groundwater discharge is important for nutrients in the oligotrophic Mediterranean (Rodellas et al., 2015; Trezzi et al., 2016). In this way, transport of fluvial materials including Fe and organic matter reach much further, here bottom nepheloid layers can generate DFe inputs from below.

Dust from the Sahara is expected to be a major source of DFe from above (Guieu et al., 1991; Guieu et al., 1997, 2010b; Spokes and Jickels, 1996; Wagener et al. 2008, 2010) as it is for Al (Rolison et al., 2015). By using Al as crustal marker Bonnet and Guieu (2006) concluded that Saharan dust is the main source for atmospheric input of DFe in the North Western Mediterranean, but according to Heimbürger et al. (2014) dust coming from the north, i.e. Europe, can also be considerable here. Although mostly considered as a source of Fe, dust can act as a sink by scavenging and/or ballasting effects (Wagener et al., 2010). Another major source for DFe might be hydrothermal activity (Lupton et al. 2011; Nomikou et al., 2013). Two volcanic systems exist in the Mediterranean, the submarine Aeolian Arc near Sicily and the Aeolian Islands and the Aegean volcanic arc around the island of Santorini (Lupton et al. 2011; Nomikou et al., 2013).

The chemistry of DFe and notably the organic complexation of DFe is essential to keep Fe that is supplied from internal cycling, as well as from external sources, in solution by enhancing its solubility and hence increasing its residence time. The concentrations of these ligands are determining how far DFe can be transported from its fluvial (Powell and Wilson-Finelli, 2003; Buck et al., 2007; Gerringa et al., 2007; Abualhaija et al., 2015; Mahmood et

al., 2015; Bundy et al., 2015), hydrothermal (Bennett et al., 2008; Sander and Koschinsky 2011; Hawkes et al., 2013; Kleint et al., 2016) and atmospheric (Wagener, et al., 2008; Rijkenberg et al., 2008) sources. Although the Fe-binding dissolved organic ligands are important, they are poorly defined and little is known about their sources and sinks (Hopkinson and Barbeau, 2007; Rijkenberg et al., 2008; Boyd et al., 2010; Gledhill and Buck, 2012). Iron-binding organic ligands are ubiquitous in the oceans and in general are more saturated with Fe in deeper waters than in surface waters. In surface waters DFe is taken up by phytoplankton, probably ligands are produced by bacteria and possibly phytoplankton, together creating a high excess ligand concentration over DFe (Gledhill et al. 2004; Gobler et al., 2004; Butler et al., 2005; Buck et al. 2010; Thuróczy et al., 2010; Poorvin et al., 2011; Gledhill and Buck, 2012; King et al. 2012; Bundy et al. 2016). Therefore, a high binding potential exists for Fe released either by mineralisation of organic material or from external Fe sources via lateral or horizontal transport.

There are only a few studies reporting research on Fe-binding dissolved organic ligands in the Mediterranean (van den Berg, 1995; Wagener et al., 2008). Van den Berg (1995) was one of the first to measure the Fe-binding ligands in the Western Mediterranean and concluded that 99% of DFe was organically complexed. He also found that the highest concentrations of Fe-binding organic ligands occurred in and just below the zone of maximum fluorescence, indicating an origin from phytoplankton and/or bacteria. Wagener et al. (2008) investigated the role of dissolved organic ligands in the dissolution of Fe from dust. The dissolution rate was linearly related to the concentration of Fe-binding dissolved organic ligands and to dissolved organic carbon (DOC). It is possible that dust is a source of ligands too (Saydam, and Senyuva, 2002; Gerringa et al., 2006) or triggers bacterial growth and the production of ligands (Wagener et al., 2008). In this research, DFe and Fe-binding dissolved organic ligands are studied in the Dutch GEOTRACES Section GA04.

2 Methods and equipment

Sampling

GEOTRACES section GA04 in the Mediterranean consisted of two legs both on board the Dutch R/V *Pelagia*. A southern cruise (S), 64PE370, started 14 May 2013 departing from Lisbon (Portugal) and ended in Istanbul (Turkey) on 05 June 2013. A northern cruise (N), 64PE374, left Istanbul on 25 July 2013 and ended in Lisbon on 11 August 2013. Figure 1 shows the cruise tracks and sampling stations.

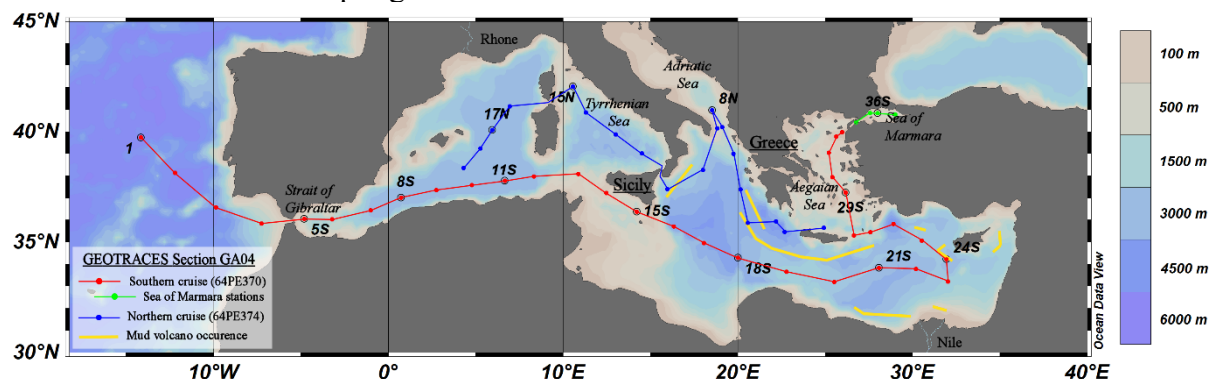


Figure 1: Cruise tracks of the Dutch GEOTRACES Section GA04 in the Mediterranean Sea. The southern cruise (S) (64PE370) is indicated with a red line and red symbols, the cruise track consists of 37 stations. The part of the southern cruise in the Sea of Marmara is indicated with a green line and green symbols. The northern cruise (N) (64PE374) is indicated with a blue line and blue symbols, it consists of 19 stations. The

stations where Fe-binding dissolved organic ligands were sampled are indicated by station numbers. Geographical names used in the main text are indicated. In yellow the occurrence of mud-volcanos is indicated where these are part of the volcanic active Hellenic and Aeolian Arcs (after Mascle et al., 2014).

During the southern cruise, 35 S stations were sampled for DFe including 10 stations sampled for Fe-binding dissolved organic ligands. Stations 1S-4S were in the Atlantic Ocean, of which station 1S was sampled for Fe-binding dissolved organic ligands. Stations 5S-33S were sampled in the Mediterranean Sea (station 25 was not sampled). Of these stations 5S, 8S, 11S, 15S, 18S, 21S, 24S and 29S were sampled for Fe-binding dissolved organic ligands. Stations 34S-36S were sampled in the Sea of Marmara. Here station 36S was sampled for Fe-binding dissolved organic ligands. During the northern cruise, stations 1N-19N were sampled for DFe, except for station 16N. Stations 8N, 13N and 17N were sampled for Fe-binding dissolved organic ligands.

The CTD-package consisted of a SeaBird SBE9plus underwater unit, an SBE11plusV2 deck unit, an SBE3plus temperature sensor, an SBE4 conductivity sensor, a Wetlabs C-Star transmissiometer (25 cm, deep, red) and an SBE43 dissolved oxygen sensor. The sensors were freshly calibrated by Seabird. In situ calibrations of the CTD-thermometers (type SBE-3) were done with a Seabird reference-thermometer (type SBE35). For the calibration of the conductivity sensor, salinity-samples were tapped on board for analysis back home. Most of the casts were tapped for Winkler titrations in order to calibrate the dissolved oxygen sensor. The Absolute Salinity (SA in g kg^{-1}) and Conservative Temperature (CT in $^{\circ}\text{C}$) have been computed using the GSW-software of TEOS-10 (IOC, SCOR, IAPSO, 2010). Density was expressed as sigma-theta, the density anomaly referenced to the surface. Fluorescence was measured as the beam attenuation coefficient at 660 nm using a Chelsea Aquatracka MKIII fluorometer. The fluorometer signal was calibrated against Chlorophyll *a* and is expressed as $\mu\text{g Chl}a \text{ dm}^{-3}$.

Water samples were taken from the ultra-clean NIOZ CTD-frame and filtered over a 0.2 μm filter using N_2 overpressure in a clean-air laboratory unit (Rijkenberg et al., 2015). Samples for DFe analysis were acidified immediately after filtration (see below). Approximately 900 mL samples were taken for the analysis of Fe-binding dissolved organic ligands. During the southern cruise these samples were stored at -18°C . Part of these were analysed on board during the northern cruise, remaining samples were analysed at the NIOZ home laboratory. Samples taken during the northern cruise were kept at 4°C in the dark and analysed on board within two days after sampling.

Figures of maps and transects were made using ODV (Schlitzer, 2016).

Analysis of the characteristics of the Fe-binding dissolved organic ligands

Competing ligand exchange adsorptive cathodic stripping voltammetry (CLE-aCSV) was performed using two systems consisting of a $\mu\text{Autolab}$ potentiationstat (Metrohm Autolab B.V.), a 663 VA stand with a Hg drop electrode (Metrohm) and a 778 sample processor with ancillary pumps and dosimats (Metrohm), all controlled using a consumer laptop running Nova 1.9 (Metrohm Autolab B.V.). For the on board measurements the VA stands were mounted on elastic-suspended plywood platforms in aluminium frames developed at the NIOZ to minimize motion-induced noise. Electrical noise reduction and backup power was provided by Fortress 750 UPS systems for spike suppression and line noise filtering (Best

Power). Sample manipulations were performed inside class 100 laminar flow hoods (Interflow B.V., the Netherlands).

The characteristics of Fe-binding dissolved organic ligands, that is both the ligand concentration $[L_t]$ (in nano-equivalents of molar Fe, nEq of M Fe) and the conditional binding constant K' (M^{-1}) with respect to $[Fe^{3+}]$, commonly expressed as $\log K'$ are determined using 2-(2-Thiazolylazo)-p-cresol (TAC) as an added measuring ligand (Croot and Johansson, 2000). TAC was used with a final concentration of 10 μM , and the complex $(TAC)_2-Fe$ was measured after equilibration (> 6 hrs). The increments of Fe concentrations used in the titration were 0 (2x), 0.2, 0.4, 0.6, 0.8, 1.0, 1.2, 1.5, 2, 2.5, 3, 4, 6, and 8 (2x) nM. Using a non-linear regression of the Langmuir isotherm, the electrical signal recorded in nA (nano-Ampere) was converted into a concentration in nM, and the ligand concentration $[L_t]$ and the binding strength K' were estimated (Gerringa et al., 2014).

Using $[L_t]$ and K' , the concentration of Fe bound to a natural Fe-binding ligand $[FeL]$, the concentration of inorganic Fe $[Fe']$ and the concentration of natural unbound ligand $[L']$ were calculated under the assumption of chemical equilibrium using:

$$DFe = [Fe^{3+}] (1 + 10^{10} + K' [L']) \quad \text{Equation 1}$$

and the ligand mass balance:

$$[L_t] = [FeL] + [L'], \quad \text{Equation 2}$$

respectively, by repeated calculations using Newton's algorithm (Press et al., 1986). The parameters from Liu and Millero (2002) were used and from these an inorganic side reaction coefficient of 10^{10} was obtained, as also determined by Hudson et al. (1992). Only during the northern cruise separate samples for determination of DFe (see below) were taken from the un-acidified Fe-binding dissolved organic ligand samples just before the analysis of the characteristics of the organic ligands. To be able to compare the results from both cruises, the DFe concentrations from immediately acidified samples were used for the calculation of the ligand characteristics. In 6 samples this DFe was either missing (4 samples) or so high that contamination was probable (2 samples). The sample taken at 501 m at station 1S was not analysed with FIA, DFe from measurements with inductively coupled plasma mass spectrometry (ICP-MS) was used instead giving comparable results (Middag et al., 2015). The other missing samples were from station 8N at 260 m, station 13N at 1000 and 1500 m, the contaminated samples were from station 13N at 100 and 2000 m depth. For these samples DFe was used which was measured in subsamples taken from the unacidified 1 L bottles just before analysis of the ligand characteristics and analysed by FIA. Earlier research showed that DFe in unacidified samples are on average 13% lower due to wall adsorption (Gerringa et al., 2015). The results of the above mentioned samples do not deviate from the general trend with depth or between stations and were thus incorporated in the results.

Table 1: Concentrations of SAFe and GEOTRACES reference samples in nM kg⁻¹. Columns show reference ID, the Intercalibration Consensus Values (ICV) and the bottle number of GS reference samples, the values measured during the cruises 64PE370 and 64PE374 in the North Atlantic Ocean, the Mediterranean Sea and the Sea of Marmara, including the standard deviation, and the number of sample analyses. SAFe S is a surface, SAFe D is deep reference sample and GS is a GEOTRACES surface and GD is a GEOTRACES deep reference sample (<http://www.geotraces.org/science/intercalibration>).

ID	ICV ± SE (nM kg ⁻¹)	Bottle nr	Measured ± SE (nM kg ⁻¹)	N
SAFe S	0.093 ± 0.008	8,47,48,76	0.067 ± 0.013	7
SAFe D2	0.933 ± 0.023	29,191	0.963 ± 0.076	2
GS	0.546 ± 0.046	12	0.836 ± 0.030	3
		141	0.493 ± 0.021	2
		154	0.736 ± 0.007	2
		186	0.541	1
		55	0.473	1
GD	1.000 ± 0.100	87,238	1.088 ± 0.102	10

The ligand characteristics were calculated with two models, one assuming the presence of one ligand class and the other assuming the presence of two ligand classes (Gerringa et al., 2014) (Supplementary Table 1). We were unable to calculate the ligand characteristics for 2 ligand classes because either only one ligand group was present, or ligand characteristics of the different ligand groups did not differ enough from each other to be distinguished as separate classes.

The side reaction coefficient α_{FeL} of the organic ligands was calculated as the product of K' and $[L']$,

$$\alpha_{FeL} = K' * [L'] = [FeL]/[Fe'], \quad \text{Equation 3}$$

α_{FeL} reflects the complexation capacity of the dissolved organic ligands to bind with Fe, which can be seen as its ability to compete for Fe with other ligands and with adsorption sites on particles. The parameter α_{FeL} is more robust to characterize the Fe-binding dissolved organic ligands than the K' and $[L']$ separately because the Langmuir equation does not treat K' and $[L']$ independently from each other. If an analytical error forces an underestimation of one, the other is automatically overestimated (Hudson et al., 2003). Moreover, in our equations, $[L']$ is, in contrast to $[L_t]$, independent of DFe (Thuróczy et al., 2010). The ratio $[L_t]/DFe$ (Supplementary Table 1 at the end of the manuscript) indicates the saturation of the ligands, which are saturated with Fe if the ratio ≤ 1 , and unsaturated when > 1 (Thuróczy et al., 2010).

Flow Injection Analysis of DFe

The DFe concentrations were measured in filtered (0.2 µm, Sartorius Sartobran 300) and acidified (pH 1.8, 2 ml/L 12M Baseline grade Seastar HCl) samples at sea using an automated Flow Injection Analysis (FIA) (Klunder et al., 2011) and described in detail by Rijkenberg et al., 2014. Samples were analysed in triplicate and average DFe concentrations and standard deviation are given in the available in the GEOTRACES GA04 database.

(<http://www.bodc.ac.uk>). The data is publicly available in August 2017 when the GEOTRACES Intermediate Data Product 2016 will be published. On average, the standard deviation of the measurements was 3.2%, generally being < 5% in samples with DFe concentrations higher than 0.1 nM. Only standard deviation (SD) of measurements near the detection limit of the system were relatively high. The average blank was determined to be at 0.033 nM during the southern cruise and 0.017 nM during the northern cruise. The blank was defined by the intercept of a low Fe sample loaded for 5, 10 and 20 seconds and was measured daily. The limit of detection, 0.019 nM during the southern cruise and 0.004 nM during the northern cruise, was defined as three times the SD of the mean of the daily measured blanks, loaded for 10 s. To better understand the day-to-day variations, a duplicate sample was measured again at least 24 hours after the first measurement. The relative differences between these measurements were of the order of 1-20%, while the largest differences were measured in samples with low DFe concentrations. To correct for this day-to-day variation, a lab standard, a sample acidified for more than 6 months, was measured daily. The consistency of the FIA system over the course of a day was verified using a drift standard. For the long-term consistency and absolute accuracy, certified SAFe and GEOTRACES reference material (Johnson et al., 2007) were measured on a regular basis (Table 1). We did not measure a consistent DFe in the GS reference samples, like we did in the other references. We do not know the cause, we might have had a contamination in two GS bottles. The DFe data have been accepted for the GEOTRACES intermediate data product 2017.

3 Hydrography

Stations 1S-4S were sampled in the Atlantic Ocean before entering the Mediterranean Sea. The Mediterranean Outflow Water (MOW) is readily recognized between 500 and 1500 m by higher salinity (>36) and lower oxygen concentrations (<200 $\mu\text{M kg}^{-1}$) (Figures 2 A, D).

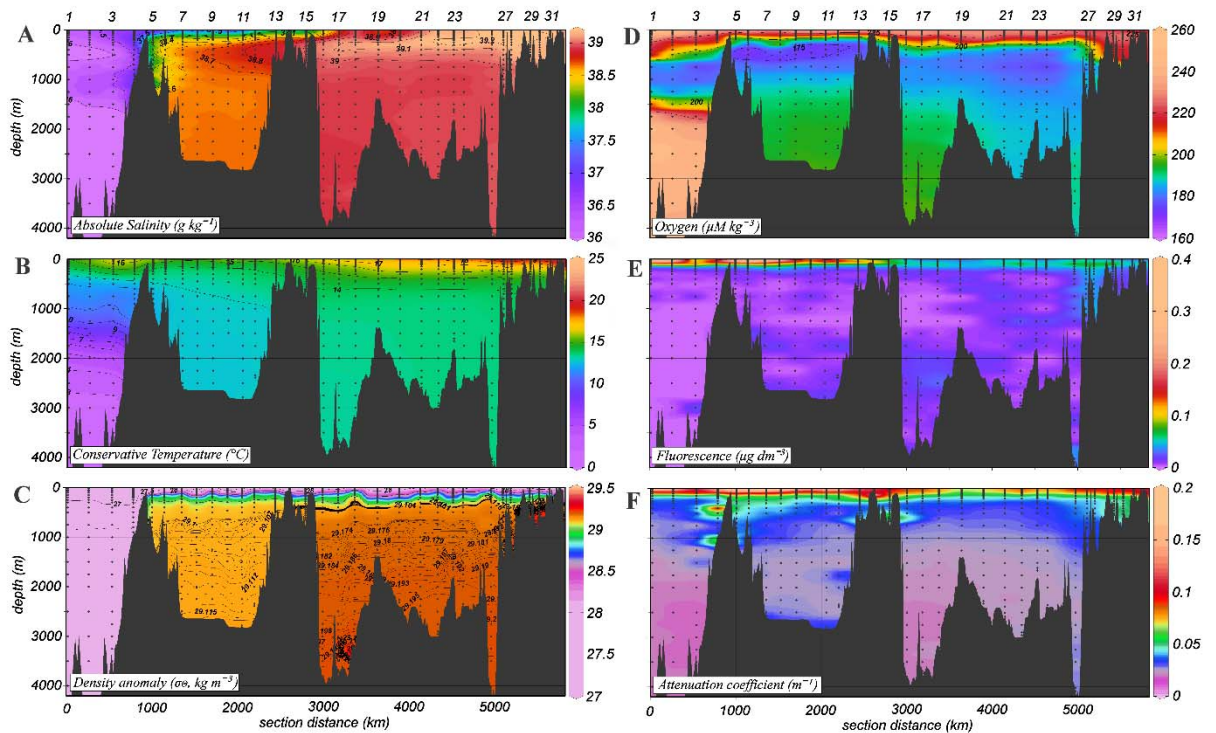


Figure 2: Southern cruise transect showing: A: Absolute Salinity (SA) in g kg^{-1} ; B: Conservative Temperature (CT) in $^{\circ}\text{C}$; C: Density as sigma-theta in kg m^{-3} ; D: Oxygen in $\mu\text{M kg}^{-3}$; E: Fluorescence in $\mu\text{g dm}^{-3}$; F: Attenuation coefficient in m^{-1} .

Salinity contours are given every 0.5 g kg⁻¹ between 36 and 37, and every 0.1 g kg⁻¹ between 37 and 39.5. Sigma-theta contours are every 0.5 kg m⁻³ between 27 and 29.5, every 0.001 kg m⁻³ between 29.1 and 29.120 and between 29.173 and 29.2 and every 0.002 kg m⁻³ between 29.2 and 29.26.

In the Mediterranean, the Atlantic Water (AW) characterized by relatively low salinity is present in the surface waters (<200 m) of especially the Western Basin. AW streams counter clockwise through the basins (e.g., Millot, 1999) and becomes warmer and more saline along its course. Formed in dense water formation areas in the Eastern Basin, the Levantine Intermediate Water (LIW) between 200 and 600 m in the southern cruise transect and 100-800 m in the northern cruise transect, streams to the west and spills into the Western Basin (see also Rolison et al., 2015). It is discernible by its relatively high salinity (>38.75 in the Eastern Basin and >38.5 in the Western Basin in the southern transect; > 38.8 in the northern transect) and in the northern transect also by its relatively high temperature (>14-14.5°C) and in the Western Basin by low oxygen (Figures 2 A, B, D, 3 A, B, D). Below LIW, three deep water masses are distinguished, the Western Mediterranean Deep Water (WMDW), the Adriatic Mediterranean Deep Water (AdMDW) and the Aegean Mediterranean Deep Water (AeMDW). The AdMDW is less saline than the AeMDW (Figure 3 A).

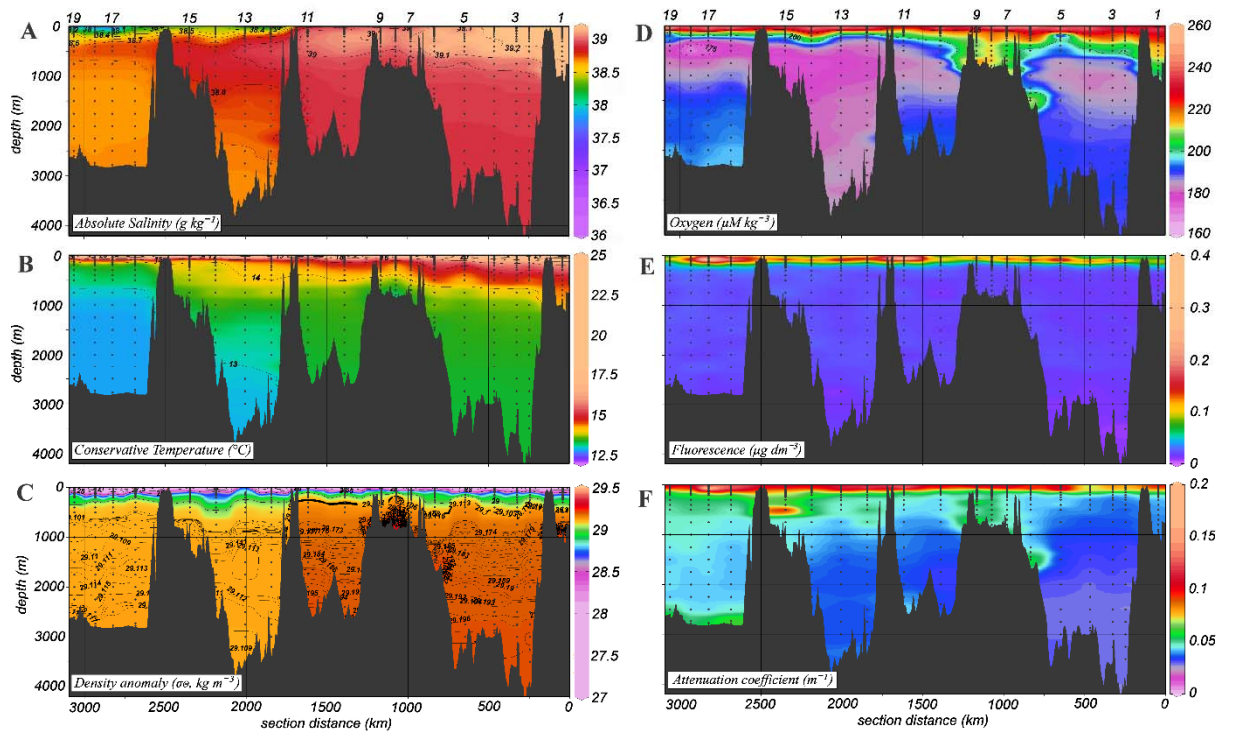


Figure 3: Northern cruise transect with A: Absolute Salinity (SA) in g kg⁻¹; B: Conservative Temperature (CT) in °C; C: Density as sigma-theta in kg m⁻³; D: Oxygen in μM kg⁻³; E: Fluorescence in μg dm⁻³; F: Attenuation coefficient in m⁻¹. Salinity contours are given every 0.1 g kg⁻¹ between 37.5 and 39.5. Sigma-theta contours are every 0.5 kg m⁻³ between 27 and 29.5, every 0.001 kg m⁻³ between 29.1 and 29.120 and between 29.173 and 29.2 and every 0.002 kg m⁻³ between 29.2 and 29.26.

Water masses are not only separated vertically, but also horizontally, due to their different formation areas. Horizontally, water masses are separated by fronts, as can be seen between AdMDW and AeMDW, for example in Figure 3C. Fronts occur around eddies (for example near stations 7N, 8N and 9N in Figure 3C, as further discussed in section 5.2 in *Deep*

high *DFe patches*), and near continental boundaries. Dynamically, horizontal transitions in density give rise to along-frontal currents, due to the rotation of the Earth, causing advective transport. Near continental boundaries and around eddies such currents are expected to be strongest with velocities ranging between 0.1 and 1 m s⁻¹ (Milot and Taupier-Letage, 2005). They become reinforced after dense water formation events, whereby density contrasts are sharpened. This gives rise to larger along-frontal currents, following vertical convection events.

The Sea of Marmara has a surface layer of about 20 m with a relatively low salinity influenced by exchange with the Black Sea ($S = 21.6$ in the east, $S = 23$ in the west) (Beşiktepe et al., 1994). This layer contains high oxygen concentrations of 213-280 $\mu\text{g kg}^{-1}$ and fluorescence is relatively high, 0.5-1.1 $\mu\text{g dm}^{-3}$ (Figure 4 A, C, E). Below a very steep pycnocline at 20 to 50 m the salinity is >38.7 and the oxygen is reduced to 10.4-18.4 $\mu\text{g kg}^{-1}$ in the east and to 20-50 $\mu\text{g kg}^{-1}$ in the west. The surface waters are transitional in character with a short residence time of months (Ünlüata et al., 1990; Beşiktepe, et al., 1994; Rank et al., 1999). Below 50 m salinity, temperature and oxygen concentrations are nearly homogeneous. According to Rank et al. (1999) the sub-halocline water is. This uniform deep water has a residence time of 6 years, which is influenced by intrusions from the Mediterranean (Rank et al., 1999, Ünlüata et al., 1990).

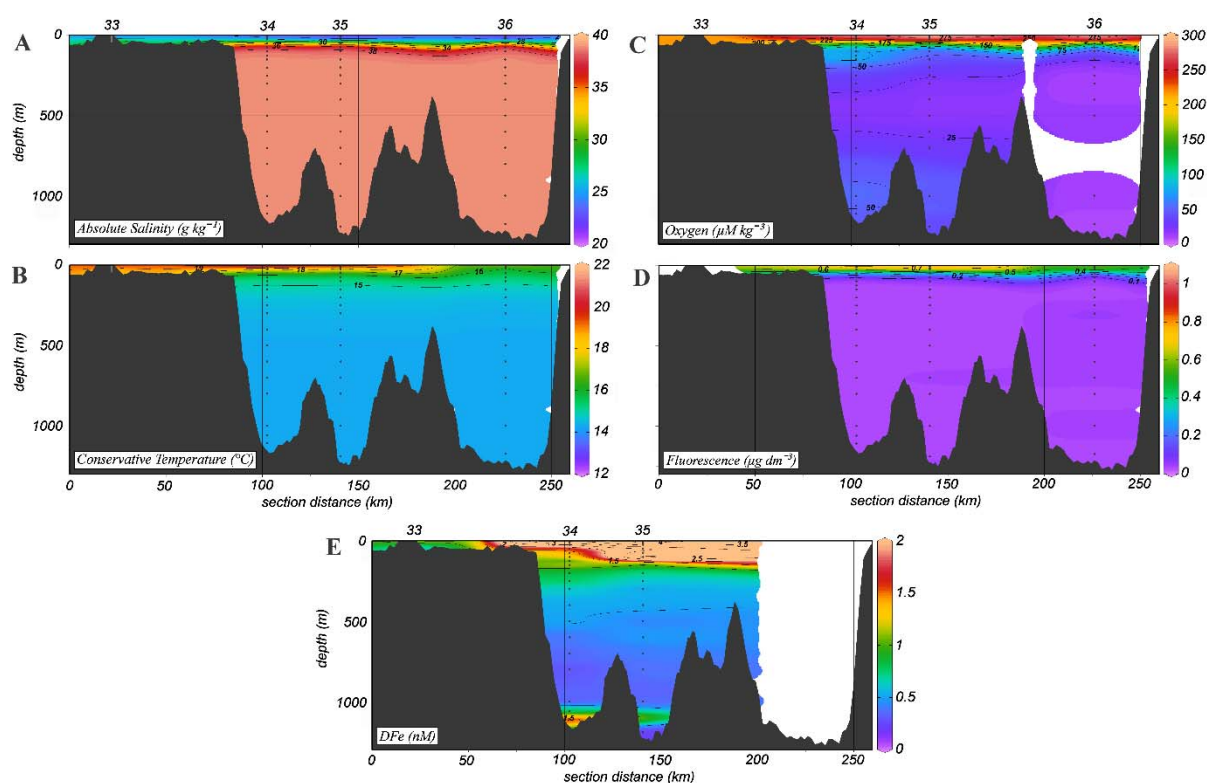


Figure 4: Transect from the Southern cruise into the Sea of Marmara with A: Absolute Salinity (SA) in g kg⁻¹; B: Conservative Temperature (CT) in °C; C: Oxygen in $\mu\text{M kg}^{-3}$; D: Fluorescence in $\mu\text{g dm}^{-3}$; E: *DFe* in nM.

There is no data available for oxygen at station 36 at 800 m, influencing the interpretation between stations by ODV.

Salinity contours are given every 2 g kg⁻¹ between 20 and 39.5.

4 Results

In the following paragraphs, median values are presented per depth layer (0-100m to show the influences of dust deposition, 100-1000 m to show properties in the LIW, and 1000-2000m and >2000m for properties of the deep water and the deepest basins, respectively) and per geographical region, the Atlantic Ocean, the Mediterranean Sea, divided in the Western Basin and the Eastern Basin, and the Sea of Marmara. Medians with interquartile ranges (IQR) were calculated instead of average because DFe and also [Lt] had maxima in deep patches, which influenced the average values and increased the standard deviations, making median values more suitable. Note that for both the Atlantic Ocean and the Sea of Marmara only one station was sampled for the Fe-binding organic ligand characteristics, and thus the number of samples (N) is rather low.

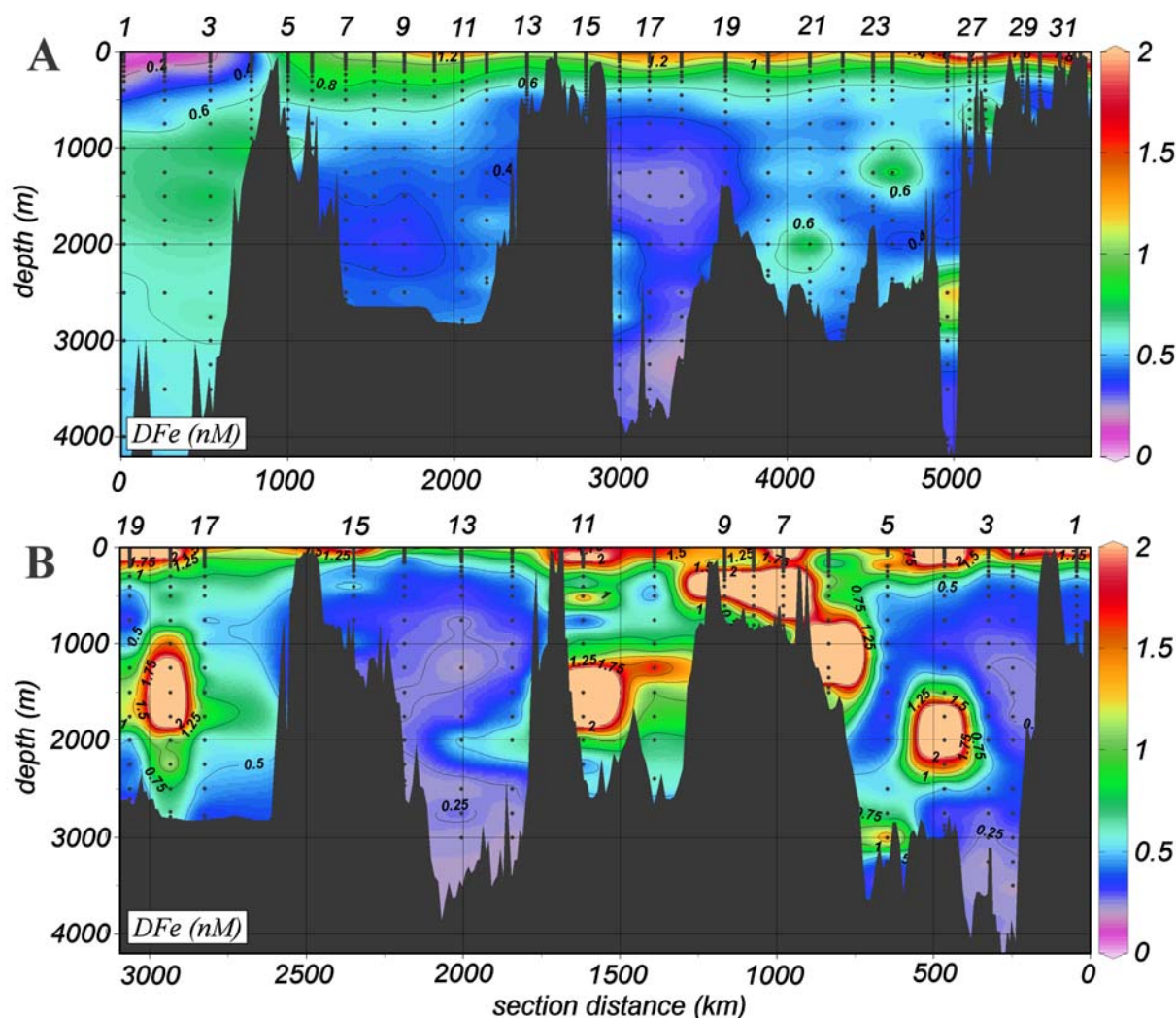


Figure 5: Southern (Figure 5A) and northern (Figure 5B) cruise transect showing DFe in nM. The southern transect consists of 721 data points, the northern transect consists of 421 data points. Station 25S was not sampled for DFe (see methods). See Figure 1 for the positions of the stations.

In the Atlantic Ocean DFe was low in the surface waters (stations 1S-4S) and ranged from 0.01 to 0.18 nM in the upper 100 m (Figure 5A). The DFe increased with depth to 0.69 nM at 1000 m in the MOW, and slightly decreased to 0.50 nM at depths larger than 3000 m at stations 1S and 2S (Figure 6A). Closer to the Mediterranean, DFe increased to 0.71-0.99 nM around 900 m (stations 3S and 4S), also in the MOW, being well below the Camarinal sill separating the Mediterranean from the Atlantic Ocean (Figures 5A, 6A).

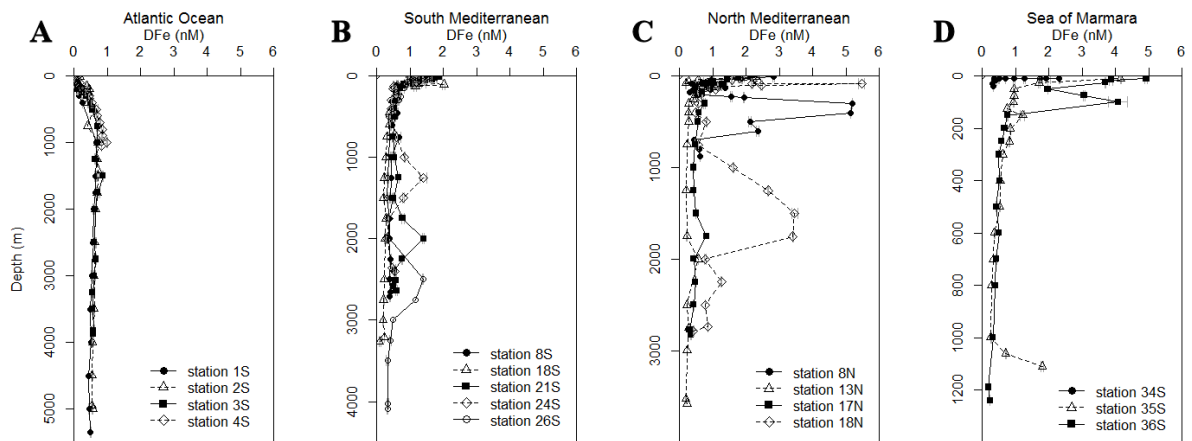


Figure 6: Dissolved Fe (DFe in nM) with standard deviations (small values falling within the size of the symbol, see Supplementary Table 1) versus depth (m) of A: stations in the Atlantic Ocean (AW); B: stations from the southern cruise (S); C: stations from the northern cruise (N); D: stations from the Sea of Marmara.

In the Mediterranean, the typical vertical profile of DFe was different from those in the Atlantic Ocean (Figures 6A versus 6B and 6C). In the Mediterranean, DFe was high near the surface (median DFe in upper 100 m = 1.4 nM, IQR = 0.96, N = 290, ranging from 0.20 to 15.35 nM), with highest near-surface DFe at stations in the north of the Eastern Basin (Figures 6B and 6C; station 27S with 15.35 nM and station 7N with 9.36 nM), decreasing to relatively low concentrations of <0.40 nM below 500-700 m (Table 2A). These deep concentrations were relatively low compared to concentrations of 0.5 nM at similar depths in the Atlantic Ocean (Rijkenberg et al., 2014, Hatta et al., 2015). The lowest deep DFe of 0.09 nM in the Mediterranean was from station 18S at 3263 m. However, very high DFe of up to 8.40 nM existed in distinct patches of both transects between 200 and 3000 m (at station 6N at 1250 m; Figure 5B). These patches were mostly found in the Eastern Basin during our northern transect, (Figure 5B). The patches varied roughly between 230-400 km in width and between 400 and 1000 m in height.

In the Sea of Marmara, DFe was elevated in the upper 100 m as in the Mediterranean and ranged between 0.94-4.93 nM. DFe decreased to 0.75-0.33 nM between 100 and 1000 m and increased close to the bottom only at one station (35S) to 1.80 nM at 1110 m (Figure 6D, Table 2A).

404 Table 2A
405

Region depth layer (m)	Atlantic Ocean			Mediterranean Sea			Western Basin			Eastern basin			Sea of Marmara		
	DFe nM	IQR	N	DFe nM	IQR	N	DFe nM	IQR	N	DFe nM	IQR	N	DFe nM	IQR	N
0-100	0.04	0.04	20	1.38	0.96	290	1.15	1.03	106	1.49	0.89	184	1.27	2.09	23
100-1000	0.38	0.42	38	0.54	0.37	472	0.57	0.41	170	0.53	0.33	302	0.52	0.28	21
1000-2000	0.67	0.07	15	0.37	0.31	120	0.40	0.19	49	0.34	0.42	71	0.47	0.76	4
>2000	0.56	0.08	21	0.35	0.24	118	0.39	0.25	47	0.34	0.25	71			

table 2B

depth layer m	N	logK' (M ⁻¹)	IQR	[Lt] (nEq of M Fe)	IQR	[L'] (nEq of M Fe)	IQR	[Lt]/DFe	IQR	Logalpha	IQR	[Fe'] (pM)	IQR
Atlantic Ocean													
0-100	2	22.06	0.44	1.13	0.35	1.10	0.35	43.4	20.5	13.07	0.29	0.03	0.01
100-1000	4	21.71	0.44	1.27	0.58	0.95	0.86	8.0	13.7	12.73	0.53	0.52	0.54
1000-2000	3	22.04	0.34	0.77	0.49	0.19	0.48	1.3	0.7	12.37	0.16	3.44	0.80
>2000	4	21.88	0.23	0.99	0.23	0.50	0.19	2.0	0.5	12.52	0.19	1.87	0.63
whole Mediterranean													
0-100	48	21.93	0.67	1.70	1.00	0.45	1.08	1.4	1.2	12.50	1.00	3.28	26.11
100-1000	61	21.78	0.58	1.30	0.82	0.67	0.97	2.2	1.6	12.61	0.57	1.64	2.39
1000-2000	14	21.89	0.54	1.32	0.58	0.83	0.86	3.3	2.5	12.69	0.44	0.84	1.10
>2000	13	21.57	0.26	1.45	0.57	1.09	0.68	4.4	2.9	12.67	0.34	0.92	0.55
East Mediterranean													
0-100	24	21.94	0.64	1.74	1.36	0.57	1.20	1.4	1.2	12.72	0.98	1.77	14.83
100-1000	24	21.66	0.52	1.51	0.82	0.89	0.84	2.7	2.0	12.49	0.23	1.99	1.27
1000-2000	8	21.55	0.41	1.61	0.43	1.24	0.70	4.0	3.4	12.54	0.41	0.92	0.84
>2000	8	21.57	0.18	1.70	0.68	1.39	0.70	4.5	2.7	12.71	0.68	1.11	11.55
West Mediterranean													
0-100	22	21.87	0.49	1.64	0.66	0.24	0.72	1.2	0.9	12.36	1.12	5.25	48.79
100-1000	39	21.87	0.64	1.21	0.80	0.55	0.83	2.0	1.7	12.72	0.63	1.42	3.09
1000-2000	6	22.13	0.27	1.02	0.35	0.37	0.59	2.5	2.7	12.84	1.60	0.68	173.00
>2000	5	21.57	0.46	1.27	0.08	0.82	0.33	3.8	2.1	12.67	0.40	0.92	0.42
Sea of Marmara													
0-100	3	21.56	0.44	2.93	2.12	0.01	0.11	0.7	0.4	10.50	1.30	1160.0	1074.8
100-1000	5	21.20	0.31	1.81	0.81	1.33	1.12	3.7	3.1	11.82	0.86	9.24	17.72
>1000	1	21.82		0.79		0.61		4.3		12.61		0.57	

406 **Table 2:** Median values per environment and per depth layer of
407 **A.** DFe with the inter quartile range (IQR) of the median and the number of samples (N);
408 **B:** ligand characteristics logK', [Lt], log α_{FeL} , the calculated [Fe'] and the ratio [Lt]/DFe with the inter
409 quartile ranges (IQR) of the median and the numbers of samples (N)
410
411
412

413 In the Atlantic Ocean, [Lt] varied between 0.54 and 2.01 nEq of M DFe (N=13, Figure
414 7A) and had a median of 1.1 nEq of M DFe in the upper 100 m, 1.3 nEq of M DFe in the
415 upper 1000 m and 0.8 and 1.0 nEq of M DFe in the 1000-2000 m below 2000 m, respectively

(Table 2B for IQR and N per depth layer). The median $\log K'$ per depth layer varied between 21.9 and 22.1 ($N = 13$). No trend with depth existed, but the values showed more variation in the upper 500 m and in the two samples taken just above the sediment (Supplementary Table 1). The [Lt] in the Mediterranean Sea varied between 0.23 and 5.51 nEq of M DFe (Figures 7B and 7C, Supplementary Table 1). $\log K'$ varied between 20.54 and 24.11. Only 17 $\log K'$ values out of 156 samples were higher than 22.5. These high values coincided with ligands that were saturated with Fe or nearly saturated as shown by the ratio [Lt]/DFe ranging between 0.6 and 2 with an average of 1.2. These high $\log K'$ values are influenced by the fact that the ligands were near saturation and therefore had very few data points in the calculation, probably resulting in a correct [Lt] but not in very reliable K' by lack of degrees of freedom. This is illustrated by the high standard errors only 5 of the 17 have an upper SE smaller than 0.4 mol^{-1} . Thus we assume that actually $\log K'$ varied between 20.54 and 22.5, although all values were used for calculating means and medians in the following text.

In the Sea of Marmara, high [Lt] up to 5.12 nEq of M DFe existed in the upper 100 m where fluorescence was high, in deeper water [Lt] varied between 0.79-2.21 nEq of M DFe; whereas $\log K'$ varied between 21.97 and 20.90 with no apparent relation with depth (Figure 7D, Table 2B).

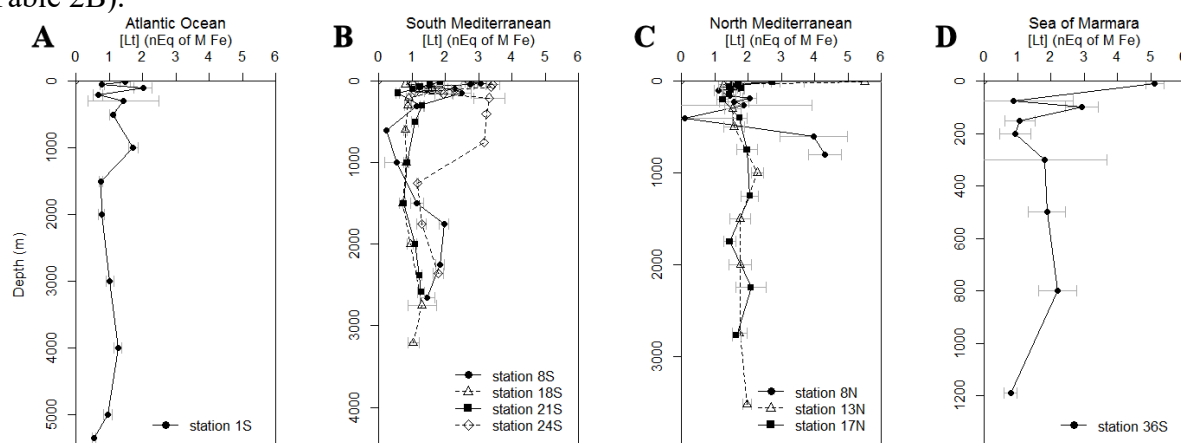


Figure 7: The concentration of Fe-binding dissolved organic ligands with standard errors ([Lt] in nEq of M Fe, small errors falling within the size of the symbol) versus depth (m) of A: stations in the Atlantic Ocean (AW); B: stations from the southern cruise (S); C: stations from the northern cruise (N); D: stations from the Sea of Marmara.

When comparing the three regions, the median DFe per depth layer increased in the Atlantic Ocean with depth and decreased with depth in the other three basins (Table 2 A). The median [Lt] per depth interval generally decreased with depth in all regions. However, in the Western Mediterranean Basin it remained almost constant with depth between 1.51 and 1.74 nEq of M Fe. (Supplementary Table 1 and Table 2B). The median [Lt] was lowest in the Atlantic Ocean (0.77-1.27 nEq of M Fe) and highest in the Sea of Marmara, ranging from 0.79 to 2.93 nEq of M Fe. The median values of [Lt] in the upper 0-100 m and 100-1000 m were higher in the Western compared to the Eastern Basin of the Mediterranean (Table 2B). The median values of $\log K'$ decreased slightly from west to east from 21.71-22.04 in the Atlantic Ocean, 21.55-21.94 in the Western Mediterranean, 21.57-22.13 in the Eastern Mediterranean to 21.2-21.82 in the Sea of Marmara.

In the Atlantic Ocean, $\log K'$ was fairly constant through the water column and ranged between 21.71 and 22.06. In the Mediterranean, both in the Western and Eastern Basins, $\log K'$ decreased with depth, with an exception between 1000 and 2000 m in the Eastern Basin where a relatively high $\log K'$ was found, 22.13 versus 21.87-21.57. In the Sea of Marmara,

log K' varied between 21.20 and 21.82 unrelated with depth. The $\text{Log}\alpha_{\text{FeL}}$ did not vary between the Atlantic Ocean and the Mediterranean Sea but was lower in the Sea of Marmara (Table 2 B). $\text{Log}\alpha_{\text{FeL}}$ decreased with depth in the Atlantic Ocean from 13.07 to 12.52, it varied little between 12.36 and 12.84 in the Mediterranean Sea and it increased with depth in the Sea of Marmara from 10.50 to 12.61. The ratio $[\text{Lt}]/\text{DFe}$ decreased with depth in the Atlantic Ocean from relatively high 43.4 in the upper 100 m to values round 1 and 2 in deep waters whereas in the other regions, the ratio increased with depth. In the Mediterranean and Sea of Marmara this ratio did not vary as much and remained between 0.7 and 4.45. Excess L decreased with depth in the Atlantic Ocean and increased with depth in the Mediterranean basins. In the Sea of Marmara excess L and DFe vary, in the surface DFe is relatively high and excess L is low (0.01-0.22 nEq of M Fe) (Figure 4, Supplementary Table 1 and Tables 2 A, 2 B).

5. Discussion

5.1 Sources and sinks of DFe and Fe-binding dissolved organic ligands in the Atlantic Ocean and the Sea of Marmara

Atlantic Ocean

The depth-profiles of DFe at stations 1S-4S were similar to those observed by others in the Atlantic Ocean, with very low concentrations near the surface due to phytoplankton uptake and scavenging by dust, although seasonal increases in DFe are reported due to dust input (Sedwick et al., 2005; Thuróczy et al., 2010; Wagener et al., 2010; Rijkenberg et al., 2012; 2014; Hatta et al., 2015, Sedwick et al., 2015). Calculated $[\text{Fe}']$ are very low 0.02-0.07 in pM in the upper 100 m, lowest values obtained in the present research. Phytoplankton uptake of Fe was probably the reason for these low values. Increasing DFe concentrations with depth in the upper 500-1000 m (Figures 5A, 6A) are probably due to the release by degradation of organic matter and the DFe decrease below 1500 m at stations 1S-3S is probably due to scavenging (Bruland et al., 2014). Below 2000 m, DFe was close to 0.5 nM as also observed by Sarthou et al. (2007). Closer to the Strait of Gibraltar (Stations 3S and 4S), DFe was higher in the MOW between 500 and 2000 m. Since the salinity and the density were also higher and the oxygen concentrations were lower at these depths (Fig 2 A,C,D), it is safe to conclude that the Mediterranean is the source of elevated DFe. Although they expected elevated DFe, Hatta et al. (2015) did not detect higher DFe in the MOW at their stations, in the same region as our stations. Also Thuróczy et al. (2010) did not detect elevated DFe in MOW at the position of our station 1S. However, at depths of the MOW Thuróczy et al. (2010) measured an increase in particulate Fe (PFe). Lenses of MOW, 'Meddies' or pulses of water are released into the Atlantic at different depths depending on density. These move with variable velocities and directions and are also dependent on season. In this way these hydrological features explain variability in DFe and it is thus not surprising that results are not overlapping here (Ambar et al., 2008).

The calculated values of $\text{log}\alpha_{\text{FeL}}$ for both the present study and that of Thuróczy et al. (2010) compare well, with values between 12.71 and 13.25 from their study and 12.05 and 13.35 from this study. In both studies ligands got more saturated with depth until 1000-2000 m, below which $[\text{Lt}]/\text{DFe}$ remained constant with depth. At our station 1S, excess L and $[\text{Fe}']$ also remained constant below 1000 m. Apparently at this depth a steady state is reached for Fe between binding by organic ligands and scavenging by marine snow (Bruland et al., 2014). The $[\text{Lt}]$ is slightly higher at 1000 m in the MOW. It is thus possible that the Mediterranean is also a source of dissolved organic Fe-binding ligands for the Atlantic Ocean. Buck et al. (2015) measured ligand characteristics East and South of the Strait of Gibraltar. They distinguished three different ligand groups with a sum $[\text{Lt}]$ around 2-3 nEq of M Fe, higher

than the concentrations at our station 1S. However, $\log\alpha_{\text{FeL}}$ was between 13 and 13.5, which is close to our values of 12.05 and 13.35. This confirms that the side reaction coefficient ($\log\alpha$) is a useful parameter for comparing results of speciation data obtained with different chemical and mathematical methods (Town and Filella, 2000; Hudson et al., 2003; Gerringa et al., 2016; Gledhill and Gerringa, submitted)

Sea of Marmara

In the Sea of Marmara the elevated DFe up to 4.93 nM was not restricted to the upper 20-50 m, the layer influenced by the outflow of the Black Sea with low salinity high oxygen and high fluorescence, but it extended over 100 m. Below 100 m DFe decreased from 1.21 to 0.18 nM. Changes in DFe are not related to changes in oxygen concentration (Figure 4 D,E). The sources of Fe are predominantly in the surface and determine the depth distribution in the upper 100 m. The sea is relatively polluted although not in Fe as concluded in sediment studies (Pekey, 2006). The sea is surrounded by land, with lateral supply from rivers like the polluted Dil Deresi, and from the Black Sea. The organic ligands at station 36S were weaker than in the Atlantic Ocean and in the Mediterranean Sea (see below). However, the lower conditional binding constants had comparable values between 20.74 and 22.2, obtained with the same method in the near-surface oxic layer of the Black Sea (Gerringa et al., 2016). The relatively high [Lt] between 1 and 2.8 nEq of M Fe in the Black Sea also compared rather well to the values between 0.79 and 5.12 nEq of M Fe in the Sea of Marmara confirming the role of the Black Sea as a source. Near the surface, the ligands were saturated at station 36S, excess L is very low and the three lowest [Lt]/DFe ratios in this research are found here; thus DFe concentrations were quite extreme if not maximum concentrations in the upper 100 m. The 100 m deep layer with elevated DFe can be explained by sinking particles, predominantly dust, releasing Fe enabled by excess L. Some of the sources for Fe, most probably rivers and the Black Sea may be important for the dissolved organic Fe-binding ligands as well. The proximity of land increases the chance that humic substances are an important part of the Fe-binding ligand pool. This ligand group might be underestimated by our method, which is not very sensitive for humic substances (Laglera et al, 2011; Abualhaija et al., 2015; Bundy et al., 2015).

5.2 Sources and sinks in the Mediterranean

As in other seas and oceans DFe and [Lt] do not systematically vary with water masses (Rijkenberg et al., 2014; Bruland et al., 2014; Gerringa et al., 2015; Buck et al., 2015; Thuróczy et al, 2011; Klunder et al., 2012). Even the LIW, considered to be an important water mass in the Mediterranean, cannot be recognized in both transects of DFe (Figures 2A, 3A and 5), as was also concluded by Rolison et al. (2015) for DA1 in the southern cruise. This most likely indicates the strong influence of vertical processes above the effect of horizontal processes. However in the West Atlantic Ocean, Gerringa et al. (2015) reported that [Lt] decreased along the flowpath of the NADW.

Near-surface waters

The high DFe concentration in the upper 100 m of the Mediterranean (Figures 5 A, B, and 6 B, C) suggests that dust is a major source of DFe, predominantly from the Sahara but also from anthropogenic sources (Guieu et al., 1991; 1997; 2010a; 2010b; Croot et al., 2004; Rijkenberg et al., 2008; Aguilar-Islas et al., 2010; Buck et al., 2010; Heimbürger et al., 2014). Guieu et al. (2010a) concluded that an increase in DFe up to 5.3 nM in the surface mixed layer in the Western Basin was due to dust input, with smaller concentrations in the Eastern

Basin. In that study, the fluxes of dust and thus metals varied strongly depending to the season and weather conditions. We found the highest DFe concentrations, close to Greece and in the Adriatic Sea. Along the southern transect, Rolison et al. (2015) also measured higher surface dissolved Al (DAI) in the Eastern Basin than in the Western Basin. River input of metals is expected to be important close to the coasts, although a large fraction of DFe and other dissolved metals may be lost by flocculation upon mixing with saline waters (Boyle et al., 1977; Sholkovitz, 1976; Paucot and Wollast, 1997; Buck et al., 2007). Lateral transport of the remaining river DFe enabled by complexation (Jones et al., 2011) is most probably occurring at such a small scale that it is hard to be distinguished by us since we sampled far from the coast along the deepest part of the Mediterranean Sea. Except for stations in the Northeast (stations 26S-33S) and near the Adriatic Sea (stations 7N, 8N, 9N) where the cruise track came relatively close to the coast and rivers and lateral transport from land could play a role as source, dust is most probably the main source for the high near-surface DFe at our station locations in the Mediterranean.

The importance of dust as source of DFe depends on the amount of dust, its Fe content and on the solubility of Fe. Fe-binding organic ligands in aerosols, like oxalate or aliphatic water soluble organic carbon compounds, increases the solubility of Fe from the dust (Paris et al., 2011; Wozniak et al., 2015). The solubility in seawater depends also on the nature of the dust particles (Visser et al., 2003; Baker and Jickells, 2006; Sedwick et al., 2007; Baker and Croot, 2010; Fishwick et al., 2014). Journet et al. (2008) found that Fe solubility of clays (illite) was even larger than that of Fe-oxides in dissolution experiments. However, also the characteristics and composition of the seawater influences Fe dissolution. Logically, it can be deduced that the solubility of Fe from dust is related to the excess ligand concentration in seawater. Indeed, Rijkenberg et al. (2008) found that the Fe-binding ligands play a key role in keeping Fe from Sahara dust in solution, as also concluded by Aguilar-Islas et al. (2010) in the Pacific and Fishwick et al. (2014) in the Sargasso Sea.

Wagener et al. (2008) found that the dissolution rates of Fe from Sahara dust were linearly related to the concentration of dissolved organic ligands in sea water. Interestingly, they discovered that excess ligands were not always successful in dissolving Fe. The dissolving capacity depended on the season and probably on the presence of freshly produced ligands by biota. Our cruises were in summer, with relatively high biological activity (Van der Poll et al., 2015). Probably the presence of freshly formed ligands enabled a high solubility of Fe (Barbeau et al., 2001). Wagener et al. (2010) concluded that successive dust depositions could have different biogeochemical reactions near the surface of the Mediterranean. They found that repetitive dust depositions in mesocosms studies had opposite effects, no flux of Fe from the dust into the seawater occurred, the opposite happened, the dust particles cleaned the water column from Fe and scavenged DFe out of the water. Sarthou and Jeandel (2001) showed that near the surface in the north of the Western Basin the exchange flux of Fe from the dissolved to the particulate phase was high, but decreased considerably with depth. According to Aguilar-Islas et al. (2010) and Fishwick et al. (2014) the dissolved Fe from dust was predominantly in the colloidal fraction. The distribution over different size fractions of Fe and the Fe-binding ligands is influencing the dissolution and residence time of Fe. This is discussed elsewhere and is outside the scope of this study (Wu et al., 2001; Croot et al., 2004; Fitzsimmons et al., 2015). Thus, DFe is the resultant of dissolution and scavenging and ballasting effects of Sahara dust. The dissolution of Fe from dust depends, apart from the nature of the dust, on the nature of the ligands (Wozniak et al., 2015; Aguilar Islas et al., 2010) and on the age of the ligands (Wagener et al., 2010), as well as on the dust history of the environment.

Even if this is not as apparent as for DFe, [Lt] is also higher near the surface (Figures 7 B, C). Sources for Fe-binding dissolved organic ligands can be biological activity (Barbeau et

al., 2001; Rue and Bruland, 1995; Gerringa et al., 2006; Gledhill et al., 2004) and in the east the Black Sea as an additional source (Gerringa et al., 2016). Due to the high DFe, the growth of phytoplankton was not limited by a lack of Fe. According to Van de Poll et al. (2015), describing the southern transect, phytoplankton was nitrate-limited in the Eastern as well as in the Western Mediterranean Sea. If there is production of siderophores it is not to relieve Fe stress, only ligands resulting from degradation and viral lysis should be formed (Poorvin et al., 2011; Slagter et al., 2016). In the Western Basin diatoms were abundant, in the Eastern Basin *Synechococcus* was most abundant. In the Western Basin chlorophyll had maximum concentrations in the upper 50 m, while in the Eastern Basin its maximum was found between 100 and 130 m (Van der Poll et al., 2015). No relationship could be detected between fluorescence and [Lt] in the southern transect. However, sample depths for DFe and [Lt] were not concentrated at the near-surface layer, the photic zone, hampering a detailed comparison of DFe and Lt versus fluorescence.

Dust is another potential source of Fe-binding ligands (Johansen et al., 2000; Saydam et al., 2002; Gerringa et al., 2006; Paris et al., 2011; Wozniak et al., 2015). Although [Lt] was relatively high in the upper 100 m, the ratio [Lt]/DFe was lowest compared to deeper waters. The ligands were not completely saturated with Fe, since the ratio was almost never below 1, as it was the case in the Sea of Marmara. The median [Lt]/DFe was 1.4 in the upper 100 m in the Western Basin and 1.15 in the Eastern Basin. The median of DFe was 0.34 nM higher in the Eastern compared to the Western Basin, whereas the median in [Lt] was only slightly, 0.1 nEq of M DFe, higher in the Eastern Basin compared to the Western Basin. Assuming that dust is the source, it is apparently not an equally important source for dissolved organic Fe-binding ligands as it is for Fe. Dust as a sink for Fe-binding ligands is as far as we know not considered, yet scavenging and ballasting of organically complexed Fe must take place since almost all DFe is complexed. We can conclude that the elevated DFe, above its inorganic solubility, near the surface of the Mediterranean Sea is possible due to the complexation by dissolved organic ligands.

Deep waters

Apart from distinct patches with elevated concentrations, which are further discussed in the next section, DFe was relatively low below 300 m along the southern transect and below 500 m along the northern transect. In most samples DFe was lower than in open oceans at similar depths. Station 18S and station 13N are good examples with deep DFe between 0.09 and 0.30 nM and 0.19 and 0.27 nM, respectively. Surface DFe inputs from Sahara dust did not impact deep waters which could be due to DFe scavenging by sinking dust itself. Wagener et al. (2010) showed that Sahara dust supply does not always increase DFe. On the contrary, they showed that through scavenging DFe can be stripped from the dissolved phase by settling dust. Due to this scavenging a direct relationship between dissolution and excess ligands is not always straightforward. It is very probable that settling dust particles scavenge Fe even though it is in its organically complexed form. Subsequently, due to the decrease of inorganic Fe (Fe') by scavenging, Fe can dissociate from the ligands, emptying the ligands over time and depth as shown by an increase in the ratio [Lt]/DFe with depth. Such an increase in the ratio indeed happened for stations 8S and 18S (Figure 8 B), but not for stations 21S and 24S which have high DFe patches at 2000 and 1250 m, respectively. Along the northern transect, an increase in the ratio was observed for stations 13N and 17N, but again not for station 8N, where high DFe patches existed (Figures 5 B, 8 C). The removal of Fe from the organic ligand complex has also been suggested by Thuróczy et al. (2011) for the Makarov Basin of the Arctic Ocean. The Arctic Ocean is far from being a dust impacted area, but due to the very long residence times of Deep Makarov Basin Water, scavenging was likely the reason for the

decrease in DFe and the simultaneous increases in $[L']$ and therefore the increase of the $[Lt]/DFe$ ratio with depth. In the present research the median of calculated concentrations of $[Fe']$ below 1000 m are close to 1 pM (0.7-1.7 pM). This is comparable to $[Fe']$ at the same

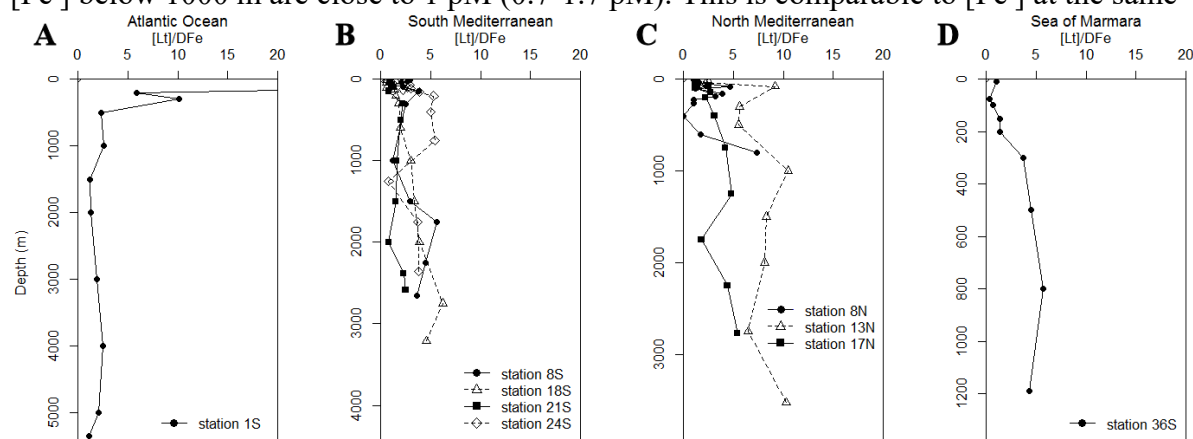


Figure 8: The ratio of Fe-binding dissolved organic ligands ($[Lt]$ in nEq of M Fe) and dissolved Fe (DFe in nM) versus depth (m) of A: stations in the Atlantic Ocean (AW); B: stations from the southern cruise (S); C: stations from the northern cruise (N); D: stations from the Sea of Marmara.

Values of samples off scale vary between 22 and 64, see supplementary table

depths for our station 1S in the Atlantic Ocean as well as in the North Western Atlantic Ocean (median 0.2-0.5 pM from three cruises in the Western Atlantic Ocean, Gerringa et al., 2015; Table 2B). Because $[Fe']$ is calculated using the ligand characteristics which depend on the analytical method (Laglera et al., 2011; Buck et al., 2012; 2016; Abualhaja et al., 2015) and on how the parameters were calculated (Laglera et al., 2013; Gerringa et al., 2014; Pižeta et al., 2015; Buck et al., 2016) we only compare our data with data collected using the same methods. The methods in this research were also applied in the Western Atlantic, Gerringa et al. (2015) concluded that $[Fe']$ between 0.2 and 1 pM represent an equilibrium or steady state concentration between complexation by organic ligands and scavenging. Only where ligands were saturated with Fe, near hydrothermal vents where DFe was relatively high, $[Fe']$ were higher. In the present research median values in the deep (>1000 m) Atlantic Ocean and Mediterranean Sea vary between 0.52 and 3.44 pM and 0.68 and 1.99 pM, respectively and are never below 0.23 pM (Supplementary table 1). According to equation 3 the values of $\log \alpha_{FeL}$ should show the same small but reversed range by a factor 3 since high α results in low $[Fe']$. Median values of $\log \alpha_{FeL}$ (values expressed with respect to Fe^{3+}) of 12.49-12.84 existed at depths >100m in Mediterranean waters, slightly higher than in the Western Atlantic Ocean with $\log \alpha_{FeL} = 13.1$ (Table 2B, Supplementary Table 1). Both the relatively small variation in $[Fe']$ and in $\log \alpha_{FeL}$ outside the deep high Fe patches indicate an equilibrium or steady state for Fe' that exist between the organic ligands and scavenging particles. At a lower $[Fe']$, Fe is so firmly bound that scavenging is hardly possible.

Deep high DFe patches

The high DFe patches could be ascribed to Fe supply by (i) lateral transport from land and shelves, (ii) vertical transport from the sediment and (iii) vertical and lateral transport from hydrothermal vents. These processes might be reflected by elevated particle densities. Particle densities can be related to the attenuation coefficient. The attenuation coefficient is high in the surface probably due to phytoplankton (Figures 2 E, F, 3 E, F). Evidence of particles elsewhere is scarce. Along the southern transect only near the Straits of Gibraltar and

Sicily, elevated attenuation coefficients coincide with slightly elevated DFe (stations 5S and 6S near 1000m depth and stations 11S and 12S at 2000 and 2500m depth, respectively).

Along the northern transect more deep patches with higher DFe were found (Figure 5 B). The attenuation coefficient is slightly higher near the bottom in the Western Basin, at station 15N, not coinciding with elevated DFe. It is also higher near the sills, especially near stations 7N, 8N and 9N (no data for station 6N exists) at the entrance of the Adriatic. The patches of elevated DFe at stations 7N, 8N and 9N are located at the southern end of the Adriatic Sea. At these stations, especially the most northern station 8N, the attenuation coefficient and oxygen are also elevated (Figure 3 D, F) and temperature is lower (Figure 3B). Elevated oxygen, higher than elsewhere in the Mediterranean, occurred also near the bottom at station 6N in the direction of the Aegean Sea at 1500 m. This is unexpected since the Adriatic Sea is known to suffer from anoxic periods (Koron et al., 2015). Elevated oxygen points to recent contact with the atmosphere and thus recently formed deep water. The attenuation coefficient is high and the temperature ($<13.5^{\circ}\text{C}$) and salinity are low. Indeed this cold water can be identified as AdMDW originating from the shallow northern Adriatic where it formed in winter (Pollak, 1951). The DFe is elevated over almost the whole water column of stations 7N, 8N and 9N except for the deep samples 100-200 m above the sediment, apparently AdMDW contains less DFe. The elevated DFe in the layer just above the AdMDW is advected by strong currents as evidenced by the large horizontal density gradients (Figure 3C). At station 8N, the ligand characteristics were analysed and the ligands were saturated at 160 and 600 m depth. In between these depths and below 600 m the [Lt]/DFe ratio was between 1.5 and 3.9, thus enabling this high solubility in almost all depths with calculated [Fe'] between 0.3 and 1 pM. At 160 and 600 m depth, the calculated [Fe'] is 231 and 316 pM above the solubility of Fe, this DFe is expected to be labile and either complexed to relatively weak dissolved organic ligands outside the detection window of our method, or present as inorganic colloids. If we assume that particles above the sediment are the source, dissolved organic ligands enable Fe to stay in the dissolved phase and explain that DFe diffused away from the source (Klunder et al. 2012; Thuróczy et al. 2011).

Highest deep DFe exists at mid depth, 0.81 nM at station 17N, 3.42 nM at station 18N and 1.35 nM at station 19N at 1750, 1750 and 1500 m, respectively. Samples from station 17N have been analysed for organic ligands. At 1750 m depth the [Lt]/DFe ratio is 1.5, and thus ligands were not saturated, enabling the high DFe of 0.81 nM. These three stations are relatively far from islands and coasts. There is no information about hydrothermal activity here that could explain this elevated DFe. Density contours below 1000 m bend downward from stations 17N and 19N to station 18N. This suggests a deep mesoscale eddy, which is the prominent feature in the mid-southern part of the Western Basin (Millot and Taupier-Letage, 2005; Schroeder et al., 2008). Apparently, DFe is transported by such an eddy. At these stations the densest water with relatively strong stratification is found below 2400 m, while the beam attenuation coefficient is only increasing in the lower 150 m above the bottom. Thus there is no indication that enhanced DFe results from deep-water formation. From our results we cannot distinguish the possible sources of DFe here.

The stations 1N-9N, 11N, 12N and 15N are closer to land and thus lateral transport from shelves and islands can be the source of DFe here. Still more than one specific source of DFe must exist to explain the multiple deep elevated DFe patches. These are mainly found between 1000 and 2500 m (Figures 5 B, 6 B, C). The depth differences indicate that not one source but at least three different sources for the three different depths are involved. From such sources the enhanced DFe spreads relatively slowly through the basins. The spreading is partially diffusive, as suggested from the form of the DFe profiles around the depths where maximum DFe is found, a gradual decrease above and below the maximum DFe. This diffusive spreading across density stratification is likely dominated by turbulence, enforced by

internal wave breaking, in the vicinity of topography (van Haren et al., 2014). Horizontally, the spreading is via boundary currents near topography and eddies further in the interior. Such eddies are observed (Figures 2 C, 3 C) in the upper 500 m nearly everywhere, but especially strong in the Adriatic Sea. These eddies can explain transport of DFe to the high DFe patches, at station 6N (1000-1500 m), stations 7N, 8N and 9N (400-800 m) stations 17N-19N (800-2500 m), and at stations 23S, 24S (1000-1500 m), 27S and 28S (near 700 m). However, density profiles do not indicate lateral transport for explaining the high DFe patches at station 4N (1500-2200 m), although between stations 4N and 5N there is a horizontal gradient, and also not at stations 10N-11N (1000-2000 m). In the Southern transect lateral transport is not supported around station 21S (near 2000 m). Therefore, either the source here is nearby or transport is in a perpendicular direction to the E-W transect. Horizontal spreading indicates deep sources, and immediately hydrothermal vents come to mind since they are known deep sources deemed to be very important (Bennett et al., 2008; Tagliabue et al., 2010; Klunder et al., 2012; Rijkenberg et al., 2014; Hatta et al., 2015). Although there are two well-known volcanic active arcs, the Hellenic Arc in the Aegean Sea and the Aeolian Arc in the Tyrrhenian Sea near Sicily, the thus far known hydrothermal activity is restricted to very shallow depths of maximum 100 m (Beaulieu et al., 2015).

Station 26S, 4100 m deep, is situated at the Rhodes depression which is 4500 m deep, nearby the Anaximander mountains of approximately 1200 m deep, also known for its mud-volcanos (Figure 1). Although, as far as we know no references exist indicating mud-volcanos as a source of DFe, mud-volcanos exist in the Mediterranean Sea at depths that coincide with the presently observed high DFe patches. For instance the Anaximander Mountains are associated with faults allowing over-pressured fluids to be erupted at the seafloor and the Amsterdam mud-volcano (at 35°19.91'N, 30°16.12'E) at 2028 m is the most active (Lazar et al., 2012). The Texel mud-volcano is located near our station 24S, at 1600 m depth (Zitter, 2004) the Kula and San Remo mud-volcanos are at 1650 m and close to our station 26S. The Milano mud-volcano is at 1900 m at 34 N, 24.8 E (Bonini and Mazzarini, 2010). The Chefren mud-volcano at 2900 m (approximately south of station 21S, but not close to this station, at 32.6° N and 28.1° E) has been identified as a potential Fe source as its porewaters have very high Fe(II) concentrations (up to 1 mM) (Omeregge et al., 2008). Also Southeast of Sicily near our station 11N mud-volcanos were discovered (Figure 1; Mascle et al., 2014).

It is conceivable that deep Fe sources can be formed by nepheloid layers, land, or due to steep topography and the sides of canyons, while most probably also mud-volcanos play a role.

6. Conclusions

The Mediterranean Sea and the Sea of Marmara have high DFe in the upper 100 m probably due to dissolution from dust. In almost all samples [Lt] was larger than DFe thus enabling the high DFe concentrations.

In the Sea of Marmara, vertical processes determined the DFe concentrations which were elevated not only in the surface 20 m but well below the strong pycnocline (22 to 38 g kg⁻¹).

Concentrations of DFe in the deep Mediterranean were either relatively low compared to the Atlantic Ocean, or relatively high in distinct patches. Deep DFe concentrations in the Mediterranean Sea were most likely low as a result of scavenging by sinking dust. This suggestion is the most probable explanation for our results and is supported by results from mesocosm experiments (Wagener et al., 2010).

The presence of distinct patches in deep waters with elevated DFe can only be explained by a combination of physical processes and sources at specific locations and depths. The

outlines of the deep high DFe patches indicate lateral transport by, for example, mesoscale eddies from deep sources. These sources are probably diverse, and can be mud-volcanos, land and deep-sea mountains. Although no previous data is known about mud-volcanos as source of Fe and no supporting data such as an increase in particle density was observed, mud-volcanos were located at coinciding depths where high DFe patches were found. In most cases in these patches the [Lt] was higher than DFe, explaining that these high dissolved concentrations can exist and be maintained for longer time.

Calculated [Fe'] in deep waters were not below 0.23 pM. Apparently this is a steady state concentration due to competition between the Fe-binding dissolved organic ligands and scavenging particles. Lower [Fe'] does exist but only in the top 100 m in the Atlantic Ocean, at our station 1S, indicating that a phytoplankton bloom can lead to lower [Fe'].

Acknowledgements

We thank Captain Pieter Kuijt and his crew of *RV Pelagia* for their hospitality and help during both cruises. The post-cruise data management by Hendrik van Aken and the data management group was excellent as usual. We thank NIOZ Marine Research Facilities for their support and everybody involved at Royal NIOZ who made this expedition possible. We also want to thank chief bottle washer Rachael Davidson who came especially from New Zealand (University of Otago) to help us cleaning the myriads of bottles in preparation of our cruises. We are grateful to the Marine Science and Technology Institute (DEU) in Turkey. Discussions on board with Kemal Can Bizsel enlightened us on the waters of our investigation. The comments of our colleague Rob Middag improved this manuscript considerably. We acknowledge the Dutch funding agency (project number: 822.01.015) of the national science foundation NWO for funding of this work as part of GEOTRACES and for funding the PhD research of author Hans Slagter (project number: 822.01.018).

The data were collected within the GEOTRACES programme and can be requested at the British Ocean Data Centre (<http://www.bodc.ac.uk>).

Data on Fe species and the dissolved Fe-binding ligands are given in the Supplementary Table 1

References

- Abualhaja, M.M., Whitby, H., van den Berg, C.M., 2015. Competition between copper and iron for humic ligands in estuarine waters. *Marine Chemistry*, 172, 46–56.
- Aguilar-Islas, A.M. Wu, J., Rember, R., Johansen, A.M., Shank, L.M., 2010. Dissolution of aerosol-derived iron in seawater: Leach solution chemistry, aerosol type, and colloidal iron fraction *Marine Chemistry* 120: 25–33 doi:10.1016/j.marchem.2009.01.011
- Ambar, I., Serra, N., Neves, F., Ferraira, T., 2008. Observations of the Mediterranean undercurrent and eddies in the Gulf of Cadiz during 2001. *J. Mar. Syst.* 71 (1–2), 195–220.
- Baker, A.R., Croot, P.L., 2010. Atmospheric and marine controls on aerosol iron solubility in seawater. *Marine Chemistry* 120, 4–13.
- Baker, A.R. and Jickells, T. D, 2006. Mineral particle size as a control on aerosol iron solubility, *Geophys. Res. Lett.*, 33, L17608, doi:10.1029/2006GL026557, 2006.
- Barbeau, K., Rue, E., Bruland, K., Butler, A., 2001. Photochemical cycling of iron in the surface ocean mediated by microbial iron (III)- binding ligands, *Nature*, 413, 409–413.

- Beaulieu, S.E., Baker, E.T., German, C.R., 2015 Where are the undiscovered hydrothermal vents on oceanic spreading ridges? *DSR II*, 121: 202–212.
- Beşiktepe, Ş., Sur, H. İ., Özsoy, E., Latif, M. A., Oğuz, T., Ünlüata, Ü., 1994. The circulation and hydrography of the Marmara Sea. *Progress in Oceanography*, 34, 285–334.
- Bennett, S.A., Achterberg, E.P., Connelly, D.P., Statham, P.J., Fones, G.R., German, C.R., 2008. The distribution and stabilisation of dissolved Fe in deep-sea hydrothermal plumes, *Earth Planet. Sci. Lett.*, 270, 157.
- Bonini, M., Mazzarini, F., 2010. Mud volcanoes as potential indicators of regional stress and pressurized layer depth. *Tectonophysics* 494, 32–47. doi:10.1016/j.tecto.2010.08.006
- Bonnet, S., Guieu, C., 2006. Atmospheric forcing on the annual iron cycle in the western Mediterranean Sea: A 1-year survey. *J. Geophys. Res.*, 111, C09010, doi:10.1029/2005JC003213.
- Boyle, E.A., Edmond, J.M., Sholkovitz, E.R., 1977. The mechanism of iron removal in estuaries. *Geochim. Cosmochim. Acta* 41: 1313–1324.
- Boyd, P.W., Iribarren, E., Sander, S.G., Hunter, K.A., and Jackson, G.A., 2010. Remineralization of upper ocean particles: implications for iron biogeochemistry. *Limnol. Oceanogr.* 55, 1271–1288.
- Bruland, K.W., Middag, R., Lohan, M.C., 2014. Controls of Trace Metals in Seawater. In: Holland, H.D., Turekian, K.K., editors. *Treatise on Geochemistry*. Oxford: Elsevier. pp. 19–51.
- Buck, K.N., Lohan, M.C., Berger, C.J.M., Bruland, K.W., 2007. Dissolved iron speciation in two distinct river plumes and an estuary: implications for riverine iron supply. *Limnol. Oceanogr.* 52, 843–855.
- Buck, C.S., Landing, W.M., Resing, J.A., Measures, C.I., 2010. The solubility and deposition of aerosol Fe and other trace elements in the North Atlantic Ocean: Observations from the A16N CLIVAR/CO2 repeat hydrography section. *Marine Chemistry* 120 (2010) 57–70. doi:10.1016/j.marchem.2008.08.003
- Buck, K.N., Moffett, J.W., Barbeau, K.A.R., Bundy, M. Kondo, Y., Wu, J., 2012. The organic complexation of iron and copper: an intercomparison of competitive ligand exchange-adsorptive cathodic stripping voltammetry (CLE-ACSV) techniques. *Limnology and Oceanography: Methods* 10: 496–515.
- Buck, K.N., Sohst, B., Sedwick, P.N., 2015. The organic complexation of dissolved iron along the U.S. GEOTRACES (GA03) North Atlantic Section. *Deep-Sea Research II* 116(2015)152–165 <http://dx.doi.org/10.1016/j.dsr2.2014.11.016>
- Buck K.N., Gerringa L.J.A., Rijkenberg M.J.A., 2016. An Intercomparison of Dissolved Iron Speciation at the Bermuda Atlantic Time-series Study (BATS) Site: Results from GEOTRACES Crossover Station A. *Front. Mar. Sci.* 3:262. doi: 10.3389/fmars.2016.00262
- Bundy, R.M., Abdulla, H.A., Hatcher, P.G., Biller, D.V., Buck, K.N. and Barbeau, K.A., 2015. Iron-binding ligands and humic substances in the San Francisco Bay estuary and estuarine-influenced shelf regions of coastal California. *Marine Chemistry*, 173, 183–194.
- Bundy, R.M., Jiang, M., Carter, M., Barbeau, K.A., 2016. Iron-binding ligands in the Southern California Current System: Mechanistic studies. *Frontiers in Marine Science* 3: Article 27.
- Butler, A., 2005. Marine siderophores and microbial iron mobilization. *Biometals* 18,369–374. doi:10.1007/s10534-005-3711-0
- Croot, P.L., Johansson, M., 2000. Determination of iron speciation by cathodic stripping voltammetry in seawater using the competing ligand 2-(2-Thiazolylazo)-p-cresol (TAC). *Electroanalysis*. 12, No.8, 565–576.

- Croot, P.L., Strey, P., Baker, A.R., 2004 Short residence time for iron in surface seawater impacted by atmospheric dry deposition from Saharan dust events. *GEOPHYS. RES. LETT.*, 31, L23S08, doi:10.1029/2004GL020153.
- Dai, M., Martin, J.-M., Cauwet, G., 1995. The significant role of colloids in the transport and transformation of organic carbon and associated trace metals (Cd, Cu and Ni) in the Rhône delta (France). *Mar. Chem.* 51: 159–175.
- de Jong, J., Schoemann, V., Lannuzel, D., Croot, P., De Baar, H., Tison, J.-L., 2012. Natural iron fertilization of the Atlantic sector of the Southern Ocean by continental shelf sources of the Antarctic Peninsula. *J. Geophys. Res.* 117, G01029, doi:10.1029/2011JG001679.
- Fishwick, M.P., Sedwick, P.N., Lohan, M.C., Worsfold, P.J., Buck, K.N., Church T.M., Ussher, S.J., 2014. The impact of changing surface ocean conditions on the dissolution of aerosol iron. *Glob. Biogeochem. Cycl.*, 28: 1235-1250.
- Fitzsimmons, J.N., Boyle, E.A., Jenkins, W.J., 2014. Distal transport of dissolved hydrothermal iron in the deep South Pacific Ocean. *PNAS* 111, 47: 16654–16661. www.pnas.org/cgi/doi/10.1073/pnas.1418778111
- Fitzsimmons, J.N., Bundy, R.M., Al-Subia, S.N., Barbeau, K.A., Boyle, E.A., 2015. The composition of dissolved iron in the dusty surface ocean: An exploration using size-fractionated iron-binding ligands. *Marine Chemistry*, 173: 125–135. doi.org/10.1016/j.marchem.2014.09.002
- Gascard, J.-C., 1973. Vertical motions in a region of deep water formation, *Deep Sea Res.*, 20, 1011– 1027.
- Gerringa, L.J.A., Veldhuis, M.J.W., Timmermans, K.R., Sarthou, G., de Baar, H.J.W., 2006. Co-variance of dissolved Fe-binding ligands with biological observations in the Canary Basin. *Mar Chem.*, 102, 276-290. doi:10.1016/j.marchem.2006.05.004
- Gerringa, L.J.A., Rijkenberg, M.J.A., Wolterbeek, H.Th., Verburg, T., Boye, M., de Baar, H.J.W., 2007. Kinetic study reveals weak Fe-binding ligand, which affects the solubility of Fe in the Scheldt estuary. *Mar Chem.* 103, 30-45. doi:10.1016/j.marchem.2006.06.002
- Gerringa, L.J.A., Rijkenberg, M.J.A., Thuróczy, C-E., Maas, L.R.M., 2014. A critical look at the calculation of the binding characteristics and concentration of iron complexing ligands in seawater with suggested improvements. *Environmental Chemistry* 11, 114-136. <http://dx.doi.org/10.1071/EN13072>.
- Gerringa, L.J.A., Rijkenberg, M.J.A., Schoemann, V., Laan, P., de Baar, H.J.W., 2015. Organic complexation of iron in the West Atlantic Ocean. *Mar Chem.* 177:434-446. doi.org/10.1016/j.marchem.2015.04.007
- Gerringa, L.J.A., Rijkenberg, M.J.A., Bown, J., Margolin, A.R., Laan, P., de Baar, H.J.W., 2016. Fe-binding dissolved organic ligands in the oxic and suboxic waters of the Black Sea. *Front. Mar. Sci.* 3:84. doi: 10.3389/fmars.2016.00084
- Gledhill, M., McCormack, P., Ussher, S., Achterberg, E.P., Mantoura, R.F.C., Worsfold, P.J., 2004. Production of siderophore type chelates by mixed bacterioplankton populations in nutrient enriched seawater incubations. *Mar.Chem.* 88: 75– 83. doi:10.1016/j.marchem.2004.03.003
- Gledhill, M., Buck, K.N., 2012. The organic complexation of iron in the marine environment: a review. *Frontiers in Microbiology* <http://dx.doi.org/10.3389/fmicb.2012.00069>.
- Gledhill, M., Gerringa, L.J.A. submitted. The effect of metal concentration on the parameters derived from complexometric titrations of trace elements in seawater – a model study. Submitted to *Frontiers in Microbiology*

- Gobler, C.J., Hutchins, D.A., Fisher, N.S., 1997. Release and bioavailability of C, N, P, Se, and Fe following viral lysis of a marine chrysophyte. *Limnol. Oceanogr.* 42,1492–1504.doi:10.4319/lo.1997.42.7.1492
- Guieu, C., Martin, J.-M., Thomas, A.J., Elbaz-Poulichet, F., 1991. Atmospheric Versus River Inputs of Metals to the Gulf of Lions. Total Concentrations, Partitioning and Fluxes. *Marine Pollution Bulletin*, Volume 22: 176-183.
- Guieu, C., Chester, R., Nimmo, M., Martin, J.-M., Guerzoni, S., Nicolas, A., Mateu, J., Keyset, S., 1997. Atmospheric input of dissolved and particulate metals to the northwestern Mediterranean. *DSR II*, 44: 655-674. PII: SO967-0645(96)00088-4
- Guieu, C., Loÿe-Pilot, M.-D., Benyahya, L., Dufour, A., 2010a. Spatial variability of atmospheric fluxes of metals (Al, Fe, Cd, Zn and Pb) and phosphorus over the whole Mediterranean from a one-year monitoring experiment: Biogeochemical implications. *Mar. Chem.*, 120: 164-178.
- Guieu, C., Dulac, F., Desboeufs, K., Wagener, T., Pulido-Villenal, E., Grisoni, J.-M., Louis, F., Ridame, C., Blain, S., Brunet, C., Bon Nguyen, E., Tran, S., Labiadh, M., Dominici, J.-M., 2010b. Large clean mesocosms and simulated dust deposition: a new methodology to investigate responses of marine oligotrophic ecosystems to atmospheric inputs. *Biogeosciences*, 7, 2765–2784. doi:10.5194/bg-7-2765-2010
- Hawkes, J.A., Connelly, D.P., Gledhill, M., Achterberg, E.P., 2013. The stabilisation and transportation of dissolved iron from high temperature hydrothermal vent systems. *Earth Plan. Sci.Lett.* 375:280–290.
- Hatta, M., Measures, C., Wu, J., Roshan, R., Fitzsimmons, J., Sedwick, P., Morton, P., 2015. An overview of dissolved Fe and Mn distributions during the 2010–2011 U.S. GEOTRACES north Atlantic cruises: GEOTRACESGA03.Deep-Sea ResearchII116(2015)117–129 <http://dx.doi.org/10.1016/j.dsr2.2014.07.005>
- Heimbürger, L.E., Migon, C., Losno, R., Miquel, J.-C., Thibodeau, B., Stabholz, M., Dufour, A., Leblond, N., 2014. Vertical export flux of metals in the Mediterranean Sea. *Deep-Sea Research I*, 87: 14–23..doi/10.1016/j.dsr.2014.02.001
- Hudson, R.J.M., Covault, D.T. Morel, F.M.M., 1992. Investigations of iron coordination and redox reactions in seawater using ⁵⁹Fe radiometry and ion-pair solvent extraction of amphiphilic iron complexes. *Mar. Chem.* 38: 209-235.
- Hudson, R.J.M., Rue, E.L., Bruland, K.W., 2003. Modeling complexometric titrations of natural water samples, *Environ. Sci. Techn.* 37, 1553.
- Hopkinson, B.M., Barbeau, K.A., 2007. Organic and redox speciation of iron in the eastern tropical North Pacific suboxic zone *Marine Chemistry* 106, 2–17. doi:10.1016/j.marchem.2006.02.008
- IOC, SCOR, IAPSO, 2010. The international thermodynamic equation of seawater – 2010: Calculation and use of thermodynamic properties. Intergovernmental Oceanographic Commission, Manuals and Guides No. 56, UNESCO, Paris, France, 196 pp.
- Johansen, A.M., Siefert, R.L., Hoffmann, M.R., 2000. Chemical composition of aerosols collected over the tropical North Atlantic Ocean. *Journal of Geophysical Research-Atmospheres* 105, 15277-15312.
- Johnson, K.S., Boyle, E., Bruland, K., Measures, C., Moffett, J., Aquilarislas, A., Barbeau, K., Cai, Y., Chase, Z., Cullen, J., Doi, T., Elrod, V., Fitzwater, S., Gordon, M., King, A., Laan, P., Laglera-Baquer, L., Landing, W., Lohan, M., Mendez, J., Milne, A., Obata, H., Osslander, L., Plant, J., Sarthou, G., Sedwick, P., Smith G.J., Sohst, B., Tanner, S., Van Den Berg, S., Wu, J., 2007. Developing standards for dissolved iron in seawater. *Eos Trans.* 88, 131.
- Jones, M.E., Beckler, J.S., Taillefert, M., 2011. The flux of soluble organic- iron(III) complexes from sediments represents a source of stable iron(III) to estuarine waters

983 and to the continental shelf. *Limnol.Oceanogr.* 56,1811–1823.
 984 doi:10.4319/lo.2011.56.5.1811
 985 Journet, E., Desboeufs, K.V., Caquineau, S., Colin, J.L., 2008. Mineralogy as a critical factor
 986 of dust iron solubility. *Geophys. Res. Lett.* 35, L07805. doi:10.1029/2007GL031589.
 987 King, A. L., Buck, K.N., Barbeau, K.A., 2012. Quasi-Lagrangian drifter studies of iron
 988 speciation and cycling off Point Conception, California. *Mar. Chem.* 128-129: 1-12.
 989 Kleint, C., Hawkes J.A., Sander S.G., Koschinsky, A., 2016. Voltammetric Investigation of
 990 Hydrothermal Iron Speciation. *Front. Mar. Sci.* 3:75. doi: 10.3389/fmars.2016.00075.
 991 Klunder, M.B., Laan, P., Middag, R., de Baar, H.J.W., van Ooijen, J.C., 2011. Dissolved Fe
 992 in the Southern Ocean (Atlantic sector). *DSR. II* 58, 2678-2694.
 993 Klunder, M. B., Laan, P., Middag, R., de Baar, H. J. W., Bakker, K., 2012. Dissolved iron in
 994 the Arctic Ocean: Important role of hydrothermal sources, shelf input and scavenging
 995 removal, *J. Geophys. Res.*, 117, C04014, doi:10.1029/2011JC007135.
 996 Koron, N., Ogrinc, N., Metzger, E., Riedel, B., Faganeli, J. 2015. The impact of reduced
 997 redox transitions on nutrient diagenesis in coastal marine sediments (Gulf of Trieste,
 998 northern Adriatic Sea). *J. Soils Sediments*: 1491-1518, DOI 10.1007/s11368-0151215-
 999 2
 1000 Laglera, L.M., Battaglia, G., Van Den Berg, C.M.G., 2011. Effect of humic substances on the
 1001 iron speciation in natural waters by CLE/CSV. *Mar. Chem.* 127, 134–143.
 1002 Laglera, L. M., Downes, J., Santos-Echeandía, J., 2013. Comparison and combined use of
 1003 linear and non-linear fitting for the estimation of complexing parameters from metal
 1004 titrations of estuarine samples by CLE/AdCSV. *Mar. Chem.* 155: 102-112.
 1005 Lazar, C.S., Parkes, R.J., Cragg, B.A., L' Haridon, S.L., Toffin, L., 2012. Methanogenic
 1006 activity and diversity in the centre of the Amsterdam Mud Volcano, Eastern
 1007 Mediterranean Sea. *FEMS Microbiol Ecol* 81, 243–254. DOI: 10.1111/j.1574-
 1008 6941.2012.01375.x
 1009 Liu, X., Millero, F.J., 2002. The solubility of iron in seawater. *Mar. Chem.* 77, 43–54.
 1010 Lupton, J., de Ronde, C., Spovieri, M., Baker, E.T., Bruno, P.P., Italiano, F., Walker, S.,
 1011 Faure, K., Leybourne, M., Britten, K., Greene, R., 2011. Active hydrothermal
 1012 discharge on the submarine Aeolian Arc. *J. Geophys. Res.*, 116, B02102,
 1013 doi:10.1029/2010JB007738.
 1014 Mahmood, A., Abualhaija, M.M., van den Berg, C.M.G., Sander, S.G., 2015. Organic
 1015 speciation of dissolved iron in estuarine and coastal waters at multiple analytical
 1016 windows. *Marine Chemistry* 177: 706–719
 1017 Mascle, J., Mary, F., Praeg, D., Brosolo, L., Camera, L., Ceramicola, S., Dupré, S., 2014.
 1018 Distribution and geological control of mud volcanoes and other fluid/free gas seepage
 1019 features in the Mediterranean Sea and nearby Gulf of Cadiz. *Geo-Marine Letters* June
 1020 2014, Volume 34, Issue 2-3, Pages 89-110.doi.org/10.1007/s00367-014-0356-4
 1021 Middag, R., Séférian, R., Conway, T.M. John, S.G., Bruland, K.W., de Baar, H.J.W., 2015.
 1022 Intercomparison of dissolved trace elements at the Bermuda Atlantic Time Series
 1023 station. *Marine Chemistry*, 177: 476–489. doi.org/10.1016/j.marchem.2015.06.014
 1024 Millot, C., 1999; Circulation in the Western Mediterranean Sea. *Journal of Marine Systems* 20
 1025 _1999. 423–442. PII: S0924- 7963 _98.00078-5
 1026 Millot, C., Taupier-Letage, I., 2005. Circulation in the Mediterranean Sea, in: *Handbook of*
 1027 *Environmental Chemistry*, vol. 5, part K, edited by A. Salot, pp. 29– 66, Springer,
 1028 New York.
 1029 Nomikou, P., Papanikolaou, D., Alexandri, M., Sakellariou, D., Rousakis, G., 2013.
 1030 Submarine volcanoes along the Aegean volcanic arc. *Tectonophysics* 597–598 (2013)
 1031 123–146. DOI: 10.1016/j.tecto.2012.10.001

- Omoregie, E.O., Mastalerz, V., de Lange, G., Straub, .L., Kappler A., Røy, H., Stadnitskaia, A., Foucher, J-P., Boetius, A., 2008. Biogeochemistry and Community Composition of Iron- and Sulfur-Precipitating Microbial Mats at the Chefren Mud Volcano (Nile Deep Sea Fan, Eastern Mediterranean). *Appl. Environm. Microbiol.*, 74, 3198–3215. doi:10.1128/AEM.01751-07
- Paris, R., Desboeufs, K.V., Journet, E., 2011. Variability of dust iron solubility in atmospheric waters: Investigation of the role of oxalate organic complexation. *Atmospheric Environment* 45, 6510-6517.
- Paucot, H., Wollast, R., 1997. Transport and transformation of trace metals in the Scheldt estuary. *Mar. Chem.* 58, 229–244.
- Pekey, H., 2006. The distribution and sources of heavy metals in Izmit Bay surface sediments affected by a polluted stream. *Marine Pollution Bulletin* 52 (2006) 1197–1208. doi:10.1016/j.marpolbul.2006.02.012
- Pollak, M.J., 1951: The sources of the deep water in the Eastern Mediterranean. *Journal of Marine Research*, 10, 128-152.
- Poorvin, L., Sander, S. G., Velasquez, Ibisani, E., Le Cleir, G. R., Wilhelm, S. W., 2011. A comparison of Fe bioavailability and binding of a catecholate siderophores with virus-mediated lysates from the marine bacterium *Vibrio alginolyticus* PWH3a. *J. Exp. Mar. Biol. Ecol.* 399, 43–47. doi: 10.1016/j.jembe.2011.01.016
- Powell, R.T., Wilson-Finelli, A., 2003. Photochemical degradation of organic iron complexing ligands in seawater. *Aquat. Sci.* 65 (2003) 367–374. DOI 10.1007/s00027-003-0679-0
- Pižeta, I., Sander, S.G., Hudson, R.J.M., Baars, O., Barbeau, K.A., Buck, K.N., Bundy R.M., Carrasco, G., Croot, P. L., Garnier, C., Gerringa, L.J.A., Gledhill, M., Hirose, K., Kondo, Y., Laglera, L.M., Nuester, J., Omanović, D., Rijkenberg, M.J.A., Takeda, S., Twining, B.S., Wells, M., 2015. Quantitative analysis of complexometric titration data: An intercomparison of methods for estimating models of metal complexation by mixtures of natural ligands. *Mar Chem*, 173: 3-24.
- Press, W.H., Flannery, B.P., Teukolsky, S.A., Vetterling, W.T., 1986. Root finding and nonlinear sets of equations, in *Numerical Recipes*, pp. 347–393 (Cambridge University Press: Cambridge, UK).
- Rodney T., Powell, R.T., Wilson-Finelli, A., 2003. Importance of organic Fe complexing ligands in the Mississippi River plume. *Est. Coast.Shelf Sci.* 58: 757–763. doi:10.1016/S0272-7714(03)00182-3
- Puig, P., Durrieu de Madron, X., Salat, J., Schroede, K., Martín, J., Karageorgis, A.P., Palanques, A., Roullier, F., Lopez-Jurado, J.L., Emelianov, M., Moutin, T., Houpert, L., 2013. Thick bottom nepheloid layers in the western Mediterranean generated by deep dense shelf water cascading. *Progress in Oceanography* 111, 1–23. doi.org/10.1016/j.pocean.2012.10.003
- Rank, D., Özsoy, E., Salihoğlu, İ., 1999. Oxygen-18, deuterium and tritium in the Black Sea and the Sea of Marmara. *Environmental Radioactivity* 43, 231-245. PII: S0265-931X(98)00094-0
- Rodellas, V., Garcia-Orellana, J., Masqué, P., Feldman, M., Weinstein, Y., 2015. Submarine groundwater discharge as a major source of nutrients to the Mediterranean Sea. *Proceedings of the National Academy of Sciences* 112, 3926-3930. doi/10.1073/pnas.1419049112
- Roether, W., Klein, B., Bruno Manca, B., Theocharis, A., Kioroglou, S., 2007. Transient Eastern Mediterranean deep waters in response to the massive dense-water output of the Aegean Sea in the 1990s. *Progress in Oceanography* 74, 540–571. doi:10.1016/j.pocean.2007.03.001

- Rolison, J.M., Middag, R., Stirling, C.H., Rijkenberg, M.J.A., de Baar, H.J.W., 2015. Zonal distribution of dissolved aluminium in the Mediterranean Sea. *Marine Chemistry* 177, Part 1, 87–100.
- Rue, E.L., Bruland, K.W., 1995. Complexation of iron(III) by natural organic ligands in the Central North Pacific as determined by a new competitive ligand equilibration/adsorptive cathodic stripping voltammetric method. *Mar. Chem.* 50, 117–138.
- Rijkenberg M.J.A., Powell C.F., Dall'Osto M., Nielsdottir M.C., Patey M.D., Hill, P.G., Baker, A.R., Jickells, T.D. Harrison, R.M., Achterberg, E.P., 2008. Changes in iron speciation following a Saharan dust event in the tropical North Atlantic Ocean. *Mar Chem* 110: 56–67.
- Rijkenberg, M. J. A., Steigenberger, S., Powell, C. F., van Haren, H., Patey, M.D., Baker, A.R., Achterberg, E.P., 2012. Fluxes and distribution of dissolved iron in the eastern (sub-) tropical North Atlantic Ocean, *Global Biogeochem. Cycles*, 26, GB3004, doi:10.1029/2011GB004264.
- Rijkenberg, M.J.A., Middag, R., Laan, P., Gerringa, L.J.A., van Aken, H., Schoemann, V., de Jong, J.T.M., de Baar, H.J.W., 2014. The distribution of dissolved iron in the West Atlantic Ocean. *PLoS ONE* 9(6): e101323. doi:10.1371/journal.pone.0101323
- Rijkenberg, M.J.A., de Baar, H.J.W., Bakker, K., Gerringa, L.J.A., Keijzer, E., Laan, M., Laan, P., Middag, R., Ober, S., Smit, M.G., 2015. “PRISTINE”, a new high volume sampler for ultraclean sampling of trace metals and isotopes. *Mar. Chem.* 177, 501–509.
- Sander, S.G., Koschinsky, A., 2011. Metal flux from hydrothermal vents increased by organic complexation. *Nat. Geosci.* 4, 145–150.
- Sarthou, G., Jeandel, C., 2001, Seasonal variations of iron concentrations in the Ligurian Sea and, iron budget in the Western Mediterranean Sea. *Mar. Chem.* 74(2-3): 115–129.
- Sarthou, G., Baker, A., Kramer, J., Laan, P., Laës, A., Ussher, S., Achterberg, E., de Baar, H.J.W., Timmermans, K.R., Blain, S., 2007. Influence of atmospheric inputs on the iron distribution in the subtropical North-East Atlantic Ocean, *Mar. Chem.*, 104, 186–202 doi:10.1016/j.marchem.2006.11.004
- Saydam, A.C., Senyuva, H.Z., 2002. Deserts: Can they be the potential suppliers of bioavailable iron? *Geophys. Res. Lett.* 29.
- Schlitzer, R., Ocean Data View, <http://odv.awi.de>, 2016.
- Schroeder, K., Taillandier, V., Vetrano, A., Gasparini, G.P., 2008. The circulation of the western Mediterranean Sea in spring 2005 as inferred from observations and from model outputs. *Deep-Sea Research I* 55, 947–965. doi:10.1016/j.dsr.2008.04.003
- Sedwick, P.N., Church, T.M., Bowie, A.R., Marsay, C.M., Ussher, S.J., Achilles, K.M., Lethaby, P.J., Johnson, R.J., Sarin, M.M., McGillicuddy, D.J., 2005 Iron in the Sargasso Sea (Bermuda Atlantic Time-series Study region) during summer: Eolian imprint, spatiotemporal variability, and ecological implications. *Glob. Biogeochem. Cycl.*, VOL. 19, 1–11. GB4006, doi:10.1029/2004GB002445.
- Sedwick, P.N., Sholkovitz, E.R., Church, T.M., 2007. Impact of anthropogenic combustion emissions on the fractional solubility of aerosol iron: evidence from the Sargasso Sea. *Geochem. Geophys. Geosyst.* 8, (10), 1–21. doi.org/10.1029/2007GC001586.
- Sedwick, P.N., Sohst, B.M., Ussher, S.J., Bowie, A.R., 2015. A zonal picture of the water column distribution of dissolved iron(II) during the U.S. GEOTRACES North Atlantic transect cruise (GEOTRACESGA03). *Deep-Sea Res. II*, 116, 166–175. <http://dx.doi.org/10.1016/j.dsr2.2014.11.004>
- Sholkovitz, E.R., 1976. Flocculation of dissolved organic and inorganic matter during the mixing of river and seawater. *Geochim. Cosmochim. Acta* 40, 831–845.

1132 Sholkovitz, E. R., 1993. The geochemistry of rare earth elements in the Amazon River
 1133 estuary. *Geochim. Cosmochim. Acta* 57, 2181–2190.
 1134 Slagter, H.A., Gerringa, L.J.A., Brussaard, C.P.D., 2016. Phytoplankton Virus Production
 1135 Negatively Affected by Iron Limitation. *Front. Mar. Sci.* 3:156. doi:
 1136 10.3389/fmars.2016.00156
 1137 Spokes, L.J., Jickells, T.D., 1996. Factors controlling the solubility of aerosol trace metals in
 1138 the atmosphere and on mixing into seawater. *Aq. Geochem.* 1, 355–374.
 1139 Tachikawa, K., Roy-Barman, M., Michard, A., Thouron, D., Yeghicheyan, D., Jeandel, C.,
 1140 2004. Neodymium isotopes in the Mediterranean Sea: Comparison between seawater
 1141 and sediment signals. *Geochim. Cosmochim. Acta*, 68, 3095–3106.
 1142 doi:10.1016/j.gca.2004.01.024
 1143 Tagliabue, A., Bopp, L., Dutay, J.C., Bowie, A.R., Chever, F., Jean-Baptiste, P., Bucciarelli,
 1144 E., Lannuzel, D., Remenyi, T., Sarthou, G., Aumont, O., Gehlen, M., Jeandel, C.,
 1145 2010. Hydrothermal contribution to the oceanic dissolved iron inventory. *Nature*
 1146 *Geoscience* 3: 252–256. DOI: 10.1038/NGEO818
 1147 Testor, P., Gascard, J.-C., 2003. Large-scale spreading of deep waters in the western
 1148 Mediterranean Sea by submesoscale coherent eddies, *J. Phys. Oceanogr.*, 33, 75– 87.
 1149 Town, R. M., and Filella, M., 2000. Dispelling the myths: Is the existence of L1 and L2
 1150 ligands necessary to explain metal ion speciation in natural waters? *Limnol. Oceanogr.*
 1151 45, 1341–1357.
 1152 Thuróczy, C.-E., Gerringa, L.J.A., Klunder, M., Middag, R., Laan, P., Timmermans, K.R., de
 1153 Baar, H.J.W., 2010. Speciation of Fe in the North East Atlantic Ocean. *DSR. I*, 57,
 1154 1444-1453.
 1155 Thuróczy, C.-E., Gerringa, L.J.A., Klunder, M., Laan, P., le Guitton, M., de Baar, H.J.W.,
 1156 2011. Distinct trends in the speciation of iron between the shelf seas and the deep
 1157 basins of the Arctic Ocean. *J. Geophys. Res.*, VOL. 116, C10009, doi:
 1158 10.1029/2010JC006835.
 1159 Trezzi, G., Garcia-Orellana, J., Rodellas, V., Santos-Exheandia, J., Tovar-Sanchez, A.,
 1160 Garcia-Solsona, E., Masque, P., 2016. Submarine groundwater discharge: A
 1161 significant source of dissolved trace metals to the North Western Mediterranean Sea.
 1162 *Mar. Chem.* 186, 90-100. doi.org/10.1016/j.marchem.2016.08.004
 1163 Ünlüata, Ü., Oğuz, T., Latif, M. A., Özsoy, E., 1990. On the physical oceanography of the
 1164 Turkish straits. In Pratt, L. J. (Ed.), *The physical oceanography of sea straits* (pp. 25-
 1165 60). NATO/ASI Series. Dordrecht: Kluwer.
 1166 Van den Berg, C.M.G., 1995. Evidence for organic complexation of iron in seawater. *Marine*
 1167 *Chemistry* 50, 139-157.
 1168 Van der Poll, W.H., Boute, P.G., Rozema, P.D., Buma, A.G.J., Kulk, G., Rijkenberg, M.J.A.,
 1169 2015. Sea surface temperature control of taxon specific phytoplankton production
 1170 along an oligotrophic gradient in the Mediterranean Sea. *Mar. Chem.* 177, 536–544.
 1171 doi.org/10.1016/j.marchem.2015.08.005
 1172 van Haren, H., Millot, C., 2009. Slantwise convection: A candidate for homogenization of
 1173 deep newly formed dense waters, *Geophys. Res. Lett.*, 36, L12604,
 1174 doi:10.1029/2009GL038736.
 1175 van Haren, H., Millot, C., Taupier-Letage, I., 2006. Fast deep sinking in Mediterranean
 1176 eddies. *Geophys. Res. Lett.*, 33, L04606, doi: 10. 1029/ 2005GL025367.
 1177 van Haren, H. et al. (ANTARES Collaboration), 2014. High-frequency internal wave motions
 1178 at the ANTARES site in the deep Western Mediterranean. *Ocean Dyn.*, 64, 507-517.
 1179 Visser, F., Gerringa, L.J.A., van der Gaast, S.J., de Baar, H.J.W., Timmermans, K.R., 2003.
 1180 The role of reactivity and iron content of aerosol dust on growth rates of two Antarctic
 1181 diatom species. *J. Phycol.* 39, 1085-1094.

- Voorhis, A. D., Webb, D. C., 1970. Large vertical currents observed in a winter sinking region of the northwestern Mediterranean, *Cah. Oceanogr.* 22, 571–580.
- Wagener, T., Pulido-Villena, E., Guieu, C., 2008. Dust iron dissolution in seawater: results from a one-year time-series in the Mediterranean Sea. *Geophys. Res. Lett.* 35, L16601.
- Wagener, T., Guieu, C., Leblond, N., 2010. Effects of dust deposition on iron cycle in the surface Mediterranean Sea: results from a mesocosm seeding experiment. *Biogeosciences* 7: 3769– 3781. Doi:10.5194/bg-7-3769-2010.
- Wozniak, A.S., Shelley, R.U., McElhemie, S.D., Landing, W.M., Hatcher, P.G., 2015. Aerosol water soluble organic matter characteristics over the North Atlantic Ocean: Implications for iron-binding ligands and iron solubility. *Marine Chemistry* 173: 162–172. doi.org/10.1016/j.marchem.2014.11.002
- Wu, J., Boyle, E., Sunda, W., Wen, L.-S., 2001. Soluble and colloidal iron in the oligotrophic North Atlantic and North Pacific. *Science* 293 (5531), 847–849.
- Zitter, T.A.C., 2004. Mud volcanism and fluid emissions in Eastern Mediterranean neotectonic zones. *Applied geology*. PhD thesis Vrije Universiteit, Amsterdam 2004, 140 pages. This is a Netherlands Research School of Sedimentary Geology (NSG) publication. ISBN 90-9017859-7

Supplementary table 1: Speciation data of the samples in which dissolved Fe-binding ligands were analysed. DFe (nM) with standard deviation (SD) of triplicate measurements. logK' and [Lt] were obtained from speciation measurements and subsequent application of the Langmuir isotherm to the obtained data (Gerringa et al., 2014). The standard errors (SE) of the data relative to the fitted curve are given. Because K' is expressed as logarithm the SE is not symmetrical and lower (down logK' SE) and upper (up logK' SE) SE are both given. The division over the species were obtained from calculations using a spreadsheet (see text in methods for more detail). NA is missing data, NA for the error in logK' means no standard error could be calculated because the fit was not good enough.

Cruise	Station	Depth	DFe	SD	logK	down. SE	up. SE	[Lt]	SE	[FeL]	[Fe']	[L']	logalpha	[L _i]/Fe
		m	nM		M ⁻¹			nEq of M Fe	M	pM	Eq of M Fe			
64PE370	1	5348	0.5	0.012	22.6	0.35	0.19	0.54	0.04	4.97E-10	2.91	4.29E-11	12.23	1.08
64PE370	1	5000	0.45	0.005	21.76	0.18	0.13	0.96	0.13	4.48E-10	1.52	5.12E-10	12.47	2.13
64PE370	1	3997	0.5	0.019	21.89	0.15	0.11	1.26	0.12	5.02E-10	0.85	7.58E-10	12.77	2.50
64PE370	1	2999	0.53	0.005	21.86	0.2	0.14	1.02	0.12	5.26E-10	1.47	4.94E-10	12.55	1.94
64PE370	1	1999	0.58	0.004	22.04	0.3	0.17	0.77	0.09	5.78E-10	2.75	1.92E-10	12.32	1.33
64PE370	1	1499	0.65	0.022	22.32	0.25	0.16	0.75	0.05	6.43E-10	2.88	1.07E-10	12.35	1.16
64PE370	1	1001	0.66	0.008	21.63	0.08	0.07	1.72	0.14	6.62E-10	1.47	1.06E-09	12.65	2.59
64PE370	1	501	0.49	NA	22.2	0.22	0.15	1.11	0.09	4.91E-10	0.50	6.19E-10	12.99	2.26
64PE370	1	300	0.14	0.002	20.94	0.55	0.24	1.43	1.07	1.41E-10	1.25	1.29E-09	12.05	10.07
64PE370	1	199	0.11	0.009	21.79	0.42	0.21	0.66	0.15	1.12E-10	0.33	5.48E-10	12.53	5.89
64PE370	1	101	0.05	0.004	21.63	0.14	0.11	2.01	0.28	4.49E-11	0.05	1.97E-09	12.92	44.67
64PE370	1	48	0.03	0.003	22.49	0.35	0.19	0.78	0.06	3.40E-11	0.01	7.46E-10	13.36	22.94
64PE370	1	9	0.02	0.001	21.62	0.1	0.08	1.47	0.16	2.30E-11	0.04	1.45E-09	12.78	63.91
64PE370	5	899	0.3	0.003	21.84	0.07	0.06	1.7	0.08	3.02E-10	0.31	1.40E-09	12.99	5.63
64PE370	5	800	0.27	0.003	21.79	0.19	0.13	0.71	0.08	2.72E-10	1.01	4.38E-10	12.43	2.60
64PE370	5	600	0.37	0.008	21.69	0.27	0.17	0.94	0.17	3.67E-10	1.31	5.73E-10	12.45	2.55
64PE370	5	400	0.75	0.017	21.78	0.21	0.14	1.42	0.17	7.48E-10	1.85	6.72E-10	12.61	1.89
64PE370	5	249	0.73	0.006	22.2	0.18	0.12	1.62	0.1	7.30E-10	0.52	8.90E-10	13.15	2.22
64PE370	5	190	0.8	0.018	21.95	0.05	0.05	2.46	0.07	8.01E-10	0.54	1.66E-09	13.17	3.07
64PE370	5	160	0.8	0.011	22	0.09	0.08	2.17	0.1	7.97E-10	0.58	1.37E-09	13.14	2.72
64PE370	5	129	0.86	0.067	21.54	0.1	0.08	1.57	0.14	8.60E-10	3.49	7.10E-10	12.39	1.82
64PE370	5	98	0.96	0.007	21.94	0.13	0.1	1.87	0.15	9.54E-10	1.20	9.16E-10	12.90	1.96
64PE370	5	69	0.99	0.035	21.78	0.18	0.13	1.37	0.2	9.83E-10	4.21	3.87E-10	12.37	1.39
64PE370	5	39	0.77	0.006	22.57	0.3	0.17	1.25	0.07	7.66E-10	0.43	4.84E-10	13.26	1.63
64PE370	5	27	1.17	0.016	22.25	0.19	0.13	1.15	0.06	1.13E-09	39.25	1.62E-11	11.46	0.98
64PE370	5	9	2.4	0.019	22.77	0.16	0.11	3.25	0.08	2.40E-09	0.48	8.50E-10	13.70	1.35
64PE370	8	2660	0.4	0.007	21.43	0.13	0.1	1.45	0.22	3.99E-10	1.41	1.05E-09	12.45	3.63

64PE370	8	2250	0.41	0.026	21.6	0.08	0.07	1.85	0.13	4.08E-10	0.71	1.44E-09	12.76	4.52
64PE370	8	1750	0.35	0.008	21.7	0.07	0.06	1.96	0.15	3.52E-10	0.44	1.61E-09	12.91	5.57
64PE370	8	1501	0.4	0.007	21.56	0.18	0.13	1.15	0.2	3.97E-10	1.45	7.53E-10	12.44	2.89
64PE370	8	1000	0.43	0.012	21.41	NA	0.37	0.53	0.35	4.14E-10	13.90	1.16E-10	11.47	1.24
64PE370	8	301	0.47	0.007	21.63	0.19	0.13	1.15	0.2	2.23E-10	1.59	6.85E-10	9.95	0.49
64PE370	8	145	0.66	0.005	21.3	0.07	0.06	2.49	0.29	6.58E-10	1.80	1.83E-09	12.56	3.77
64PE370	8	98	1.02	0.016	21.54	0.07	0.06	2.27	0.2	1.01E-09	2.33	1.26E-09	12.64	2.23
64PE370	8	71	1.18	0.028	21.51	0.18	0.12	1.13	0.16	1.09E-09	86.14	3.91E-11	11.10	0.96
64PE370	8	42	1.3	0.041	22.03	0.07	0.06	2.76	0.09	1.30E-09	0.83	1.46E-09	13.19	2.12
64PE370	8	27	1.15	0.032	21.48	0.05	0.04	3.06	0.17	1.14E-09	1.98	1.92E-09	12.76	2.67
64PE370	8	10	0.96	0.023	21.93	0.13	0.1	2.79	0.19	9.57E-10	0.61	1.83E-09	13.19	2.91
64PE370	11	2781	0.41	0.007	21	NA	0.54	0.47	1.33	3.70E-10	37.00	1.00E-10	11.00	1.15
64PE370	11	2250	0.34	0.015	21.89	NA	0.39	0.23	0.12	2.27E-10	116.52	2.52E-12	10.29	0.67
64PE370	11	1751	0.41	0.012	21.94	0.21	0.14	1.34	0.16	4.13E-10	0.51	9.27E-10	12.91	3.24
64PE370	11	1252	0.51	0.019	21.9	0.11	0.09	1.41	0.11	5.07E-10	0.71	9.03E-10	12.86	2.78
64PE370	11	751	0.54	0.013	22.06	0.26	0.16	0.76	0.09	5.42E-10	2.16	2.18E-10	12.40	1.40
64PE370	11	400	0.68	0.014	22.61	0.64	0.25	0.68	0.06	6.67E-10	12.30	1.33E-11	11.73	1.00
64PE370	11	200	1	0.026	22.25	0.33	0.18	0.99	0.1	9.69E-10	26.54	2.05E-11	11.56	0.99
64PE370	11	146	0.76	0.003	22.05	0.26	0.16	0.89	0.1	7.56E-10	5.03	1.34E-10	12.18	1.17
64PE370	11	100	0.88	0.014	22.29	0.35	0.19	0.84	0.09	8.30E-10	44.56	9.56E-12	11.27	0.96
64PE370	11	71	0.89	0.021	22.83	0.94	0.28	0.98	0.09	8.84E-10	1.36	9.64E-11	12.81	1.11
64PE370	11	53	1.29	0.029	24.11	NA	0.62	1.33	0.05	1.29E-09	0.28	3.63E-11	13.67	1.03
64PE370	11	40	1.41	0.033	22.27	0.61	0.24	1.51	0.25	1.40E-09	7.04	1.07E-10	12.30	1.07
64PE370	11	10	2.57	0.092	21.93	0.17	0.12	2.29	0.16	2.28E-09	287.33	9.33E-12	10.90	0.89
64PE370	15	610	0.42	0.014	21.7	0.33	0.19	0.76	0.19	4.13E-10	2.37	3.47E-10	12.24	1.83
64PE370	15	524	0.35	0.028	21.92	0.07	0.06	1.42	0.06	3.50E-10	0.39	1.07E-09	12.95	4.06
64PE370	15	445	0.41	0.009	22.06	0.17	0.12	1.65	0.13	4.07E-10	0.28	1.24E-09	13.15	4.05
64PE370	15	365	0.42	0.017	21.87	0.27	0.17	1.36	0.2	4.23E-10	0.61	9.37E-10	12.84	3.21
64PE370	15	284	0.55	0.013	21.95	0.28	0.17	1.21	0.15	5.52E-10	0.94	6.58E-10	12.77	2.19
64PE370	15	205	0.55	0.001	22.13	0.14	0.11	1.26	0.08	5.52E-10	0.58	7.08E-10	12.98	2.28
64PE370	15	160	0.63	0.019	21.98	0.13	0.1	1.5	0.1	6.30E-10	0.76	8.70E-10	12.92	2.38
64PE370	15	130	0.71	0.011	22.08	0.3	0.18	1.13	0.12	7.04E-10	1.37	4.26E-10	12.71	1.60
64PE370	15	100	0.68	0.021	21.28	0.17	0.12	1.14	0.22	6.70E-10	7.47	4.70E-10	11.95	1.68
64PE370	15	70	0.69	0.01	21.76	0.16	0.12	1.29	0.13	6.90E-10	2.00	6.00E-10	12.54	1.86
64PE370	15	39	1.53	0.039	22.02	0.19	0.13	1.73	0.2	1.52E-09	6.84	2.12E-10	12.35	1.13
64PE370	15	10	1.56	0.018	22.16	0.12	0.09	1.93	0.08	1.55E-09	2.86	3.76E-10	12.74	1.24
64PE370	18	3210	0.22	0.007	21.57	0.14	0.11	1.04	0.17	2.23E-10	0.74	8.17E-10	12.48	4.64

64PE370	18	2750	0.21	0.009	21.28	0.26	0.16	1.3	0.43	2.09E-10	1.01	1.09E-09	12.32	6.19
64PE370	18	1999	0.24	0.011	22.12	0.23	0.15	0.95	0.09	2.43E-10	0.26	7.07E-10	12.97	3.91
64PE370	18	1499	0.21	0.011	22.14	0.17	0.12	0.71	0.1	2.05E-10	0.29	5.05E-10	12.84	3.46
64PE370	18	1000	0.27	0.013	21.93	0.15	0.11	0.82	0.08	2.71E-10	0.58	5.49E-10	12.67	3.01
64PE370	18	600	0.39	0.011	22.74	0.75	0.26	0.8	0.06	3.90E-10	0.17	4.10E-10	13.35	2.05
64PE370	18	300	0.49	0.023	21.68	0.14	0.11	0.88	0.1	4.85E-10	2.57	3.95E-10	12.28	1.80
64PE370	18	205	0.62	0.016	22.28	0.26	0.16	0.91	0.08	6.20E-10	1.12	2.90E-10	12.74	1.47
64PE370	18	125	1.16	0.037	21.6	0.16	0.12	1.62	0.25	1.15E-09	6.18	4.68E-10	12.27	1.40
64PE370	18	101	2.01	0.035	23.21	NA	0.82	1.21	0.11	1.21E-09	802.09	9.30E-14	10.18	0.60
64PE370	18	80	1.41	0.067	22.52	0.17	0.12	1.6	0.06	1.40E-09	2.17	1.95E-10	12.81	1.14
64PE370	18	41	1.41	0.052	22.51	NA	NA	0.8	NA	8.00E-10	612.40	4.03E-13	10.12	0.57
64PE370	18	9	1.6	0.035	22.05	0.85	0.27	1.02	0.16	1.02E-09	581.56	1.56E-12	10.24	0.64
64PE370	21	2587	0.51	0.013	22.01	0.15	0.11	1.27	0.11	5.08E-10	0.65	7.62E-10	12.89	2.50
64PE370	21	2380	0.53	0.033	22.1	0.13	0.1	1.22	0.08	5.31E-10	0.61	6.89E-10	12.94	2.29
64PE370	21	2000	1.4	0.029	22.33	0.27	0.16	1.09	0.06	1.09E-09	312.63	1.63E-12	10.54	0.78
64PE370	21	1500	0.51	0.034	22.55	0.29	0.17	0.75	0.04	5.09E-10	0.60	2.41E-10	12.93	1.47
64PE370	21	1000	0.54	0.022	22.35	0.22	0.15	0.85	0.06	5.35E-10	0.76	3.15E-10	12.85	1.59
64PE370	21	501	0.54	0.014	21.87	0.15	0.11	1.09	0.1	5.40E-10	1.32	5.50E-10	12.61	2.01
64PE370	21	301	0.6	0.012	22.11	0.09	0.07	1.3	0.06	6.02E-10	0.67	6.98E-10	12.95	2.16
64PE370	21	146	0.72	0.006	22.95	NA	0.43	0.57	0.05	5.70E-10	146.44	4.36E-13	10.59	0.80
64PE370	21	101	0.82	0.006	22.48	0.33	0.19	1.02	0.07	8.18E-10	1.34	2.02E-10	12.79	1.25
64PE370	21	70	1.15	0.018	22.93	0.48	0.22	1.24	0.05	1.15E-09	1.49	9.05E-11	12.89	1.08
64PE370	21	40	1.67	0.023	22.56	0.43	0.21	1.53	0.08	1.53E-09	139.03	3.03E-12	11.04	0.92
64PE370	21	10	1.87	0.087	21.98	0.14	0.11	1.86	0.12	1.82E-09	50.66	3.77E-11	11.56	0.99
64PE370	24	2355	0.47	0.027	21.55	0.1	0.08	1.79	0.16	4.65E-10	0.99	1.32E-09	12.67	3.84
64PE370	24	1749	0.35	0.008	21.87	0.2	0.14	1.29	0.14	3.49E-10	0.50	9.41E-10	12.84	3.69
64PE370	24	1250	1.4	0.095	21.97	NA	0.5	1.17	0.02	1.16E-09	230.42	5.42E-12	10.70	0.84
64PE370	24	750	0.59	0.025	21.54	0.06	0	3.17	0	5.91E-10	0.66	2.58E-09	12.95	5.35
64PE370	24	400	0.64	0.034	21.25	0.07	0	3.23	0	6.40E-10	1.39	2.59E-09	12.66	5.04
64PE370	24	205	0.63	0.003	21.17	0.09	0.07	3.32	0.48	6.23E-10	1.56	2.70E-09	12.60	5.31
64PE370	24	160	0.5	0.015	20.85	0.93	0.27	1.95	0.27	4.97E-10	4.83	1.45E-09	12.01	3.88
64PE370	24	130	0.5	0.006	22.05	0.17	0	1.1	0	5.03E-10	0.75	5.97E-10	12.83	2.18
64PE370	24	114	0.62	0.001	21.28	0.06	0	1.89	0	6.18E-10	2.55	1.27E-09	12.38	3.04
64PE370	24	100	0.83	0.001	21.79	0.08	0.06	2.29	0.12	8.33E-10	0.93	1.46E-09	12.95	2.75
64PE370	24	70	1.18	0.033	21.66	0.06	0	3.37	0	1.18E-09	1.18	2.19E-09	13.00	2.85
64PE370	24	40	1.4	0.025	21.78	0.09	0.07	3.42	0.21	1.40E-09	1.15	2.02E-09	13.09	2.45
64PE370	24	9	1.63	0.027	21.44	0.08	0.07	2.72	0.23	1.62E-09	5.38	1.10E-09	12.48	1.67

64PE370	29	501	0.3	0.008	21.66	0.09	0.08	1.47	0.13	2.98E-10	0.56	1.17E-09	12.73	4.92
64PE370	29	400	0.3	0.002	22.28	0.23	0.15	0.76	0.07	2.99E-10	0.34	4.61E-10	12.94	2.54
64PE370	29	300	0.35	0.002	22.14	0.35	0.19	0.64	0.08	3.47E-10	0.86	2.93E-10	12.61	1.84
64PE370	29	200	0.38	0.002	21.44	0.34	0.19	0.75	0.23	3.78E-10	3.70	3.72E-10	12.01	1.96
64PE370	29	150	0.5	0.013	22.81	NA	0.31	0.77	0.07	4.96E-10	0.28	2.74E-10	13.25	1.55
64PE370	29	100	0.59	0.031	22.34	0.18	0.13	0.64	0.04	5.81E-10	4.54	5.85E-11	12.11	1.09
64PE370	29	79	0.72	0.026	21.94	0.34	0.19	0.99	0.15	7.19E-10	3.05	2.71E-10	12.37	1.37
64PE370	29	70	0.92	0.007	21.44	0.12	0.09	1.73	0.24	9.18E-10	4.10	8.12E-10	12.35	1.88
64PE370	29	40	1.67	0.021	22.09	0.15	0.11	1.68	0.1	1.64E-09	30.97	4.30E-11	11.72	1.01
64PE370	36	1190	0.18	0.002	21.82	0.69	0.25	0.79	0.2	1.83E-10	0.45	6.07E-10	12.60	4.32
64PE370	36	801	0.39	0.002	21.23	0.16	0.11	2.21	0.57	3.86E-10	1.25	1.82E-09	12.49	5.71
64PE370	36	500	0.42	0.004	21.35	0.31	0.18	1.88	0.56	4.15E-10	1.26	1.47E-09	12.52	4.52
64PE370	36	300	0.49	0.004	20.7	1.14	0.28	1.81	1.88	4.87E-10	7.34	1.32E-09	11.82	3.66
64PE370	36	200	0.67	0.001	21.2	0.69	0.25	0.92	0.47	6.54E-10	15.47	2.66E-10	11.63	1.38
64PE370	36	150	0.75	0.017	20.92	0.32	0.18	1.07	0.46	7.27E-10	25.43	3.43E-10	11.46	1.42
64PE370	36	100	4.08	0.279	21.56	0.41	0.21	2.93	0.5	2.92E-09	1156.96	6.96E-12	10.40	0.72
64PE370	36	75	3.06	0.028	21.09	NA	0.69	0.89	1.79	8.87E-10	2173.32	3.32E-12	9.61	0.29
64PE370	36	9	4.93	0.039	21.97	0.16	0.12	5.12	0.28	4.91E-09	24.50	2.15E-10	12.30	1.04
64PE374	8	801	0.59	0.001	21.1	0.06	0.05	4.31	0.5	5.92E-10	1.26	3.72E-09	12.67	7.27
64PE374	8	600	2.35	0.034	20.91	0.13	0.1	3.97	1.01	2.33E-09	17.52	1.64E-09	12.12	1.69
64PE374	8	260	1.85	NA	20.72	NA	0.32	1.87	2.04	1.68E-09	169.24	1.89E-10	11.00	1.01
64PE374	8	220	1.56	0.033	21.4	0.4	0.21	1.57	0.44	1.49E-09	72.13	8.21E-11	11.31	1.01
64PE374	8	190	0.64	0.004	21.65	0.13	0.1	2.05	0.2	6.39E-10	1.01	1.41E-09	12.80	3.20
64PE374	8	160	0.37	0.003	21.7	0.17	0.12	1.45	0.17	3.69E-10	0.68	1.08E-09	12.73	3.92
64PE374	8	130	1.38	0.002	21.7	NA	NA	0.29	NA	3.73E-10	0.69	1.08E-09	12.73	3.88
64PE374	8	101	0.95	0.009	22.76	NA	0.44	1.12	0.15	9.46E-10	0.95	1.74E-10	13.00	1.18
64PE374	8	79	0.36	0.002	21.65	0.11	0.09	1.71	0.15	3.61E-10	0.60	1.35E-09	12.78	4.72
64PE374	8	40	0.98	0.002	21.8	0.19	0.13	1.5	0.16	9.78E-10	2.97	5.22E-10	12.52	1.53
64PE374	8	8	2.84	0.024	21.62	0.15	0.11	2.7	0.25	2.66E-09	172.94	3.69E-11	11.19	0.95
64PE374	13	3526	0.19	0.002	21.54	0.07	0.06	1.97	0.14	1.91E-10	0.31	1.78E-09	12.79	10.31
64PE374	13	2750	0.27	0.002	21.6	0.12	0.09	1.75	0.22	2.71E-10	0.46	1.48E-09	12.77	6.46
64PE374	13	2000	0.22	NA	21.27	0.12	0.1	1.77	0.34	2.18E-10	0.76	1.55E-09	12.46	8.08
64PE374	13	1500	0.21	NA	21.34	0.16	0.12	1.76	0.31	2.12E-10	0.63	1.55E-09	12.53	8.26
64PE374	13	1000	0.22	NA	21.37	0.07	0	2.28	0.19	2.18E-10	0.45	2.06E-09	12.68	10.46
64PE374	13	499	0.29	0.002	21.28	0.16	0.12	1.57	0.31	2.86E-10	1.17	1.28E-09	12.39	5.47
64PE374	13	300	0.28	0.006	21.46	0.14	0.1	1.54	0.25	2.75E-10	0.75	1.26E-09	12.56	5.58
64PE374	13	205	0.47	0.002	21.41	0.14	0.11	1.47	0.22	4.69E-10	1.82	1.00E-09	12.41	3.12

64PE374	13	125	0.51	0.016	21.24	0.16	0.12	2.06	0.44	5.04E-10	1.86	1.56E-09	12.43	4.07
64PE374	13	100	0.35	NA	21.22	0.07	0.06	2.65	0.28	3.48E-10	0.91	2.30E-09	12.58	7.59
64PE374	13	80	0.19	0.003	21.82	0.12	0.09	1.76	0.14	1.91E-10	0.18	1.57E-09	13.02	9.21
64PE374	13	40	0.57	0.003	21.83	0.24	0.15	1.28	0.16	5.70E-10	1.19	7.10E-10	12.68	2.24
64PE374	13	8	2.3	0.01	20.54	0.19	0.13	5.51	2.81	2.28E-09	20.40	3.23E-09	12.05	2.39
64PE374	17	2774	0.31	0.013	21.71	0.1	0.08	1.65	0.13	3.05E-10	0.44	1.35E-09	12.84	5.41
64PE374	17	2249	0.48	0.006	21.45	0.24	0.15	2.09	0.45	4.76E-10	1.05	1.61E-09	12.66	4.38
64PE374	17	1749	0.81	0	21.54	0.15	0.11	1.45	0.18	8.06E-10	3.61	6.44E-10	12.35	1.79
64PE374	17	1250	0.43	0.017	21.33	0.1	0.08	2.05	0.26	4.24E-10	1.22	1.63E-09	12.54	4.82
64PE374	17	749	0.47	0.01	21.5	0.18	0.13	1.97	0.32	4.68E-10	0.99	1.50E-09	12.68	4.20
64PE374	17	400	0.57	0.002	21.5	0.14	0.1	1.74	0.22	5.68E-10	1.53	1.17E-09	12.57	3.05
64PE374	17	200	0.56	0.011	21.73	0.22	0.15	1.24	0.17	5.62E-10	1.55	6.78E-10	12.56	2.20
64PE374	17	145	0.54	0.004	21.56	0.16	0.12	1.43	0.2	5.35E-10	1.65	8.95E-10	12.51	2.66
64PE374	17	100	1.26	0.004	21.71	0.36	0.19	1.49	0.28	1.25E-09	10.01	2.43E-10	12.10	1.19
64PE374	17	75	0.72	0.005	22.25	0.19	0.13	1.79	0.11	7.24E-10	0.38	1.07E-09	13.28	2.47
64PE374	17	65	1.02	0.004	22.34	0.24	0.15	1.44	0.09	1.02E-09	1.12	4.18E-10	12.96	1.41
64PE374	17	41	1.43	0.004	22.54	0.42	0.21	1.71	0.11	1.43E-09	1.47	2.80E-10	12.99	1.19
64PE374	17	10	2.14	0	20.83	0.2	0.14	2.74	0.95	2.09E-09	47.51	6.51E-10	11.64	1.28

1210

1211

1212